



Optimized reaction mechanism rate rules for ignition of normal alkanes

Title	Optimized reaction mechanism rate rules for ignition of normal alkanes
Author(s)	Cai, Liming;Pitsch, Heinz;Mohamed, Samah Y.;Raman, Venkat;Bugler, John;Curran, Henry J.;Sarathy, S. Mani
Publication Date	2016-08-10
Publisher	Elsevier
Repository DOI	10.1016/j.combustflame.2016.04.022

Optimized reaction mechanism rate rules for ignition of normal alkanes

Liming Cai^{a,*}, Heinz Pitsch^a, Samah Y. Mohamed^b, Venkat Raman^c, John Bugler^d, Henry Curran^d, S. Mani Sarathy^b

^a*Institute for Combustion Technology, RWTH Aachen University, 52062 Aachen, Germany*

^b*Clean Combustion Research Center, King Abdullah University of Science and Technology, Thuwal 23955-6900, Saudi Arabia*

^c*Department of Aerospace Engineering, University of Michigan, Ann Arbor 48109, USA*

^d*Combustion Chemistry Centre, National University of Ireland, Galway, Ireland*

Abstract

The increasing demand for cleaner combustion and reduced greenhouse gas emissions motivates research on the combustion of hydrocarbon fuels and their surrogates. Accurate detailed chemical kinetic models are an important prerequisite for high fidelity reacting flow simulations capable of improving combustor design and operation. The development of such models for many new fuel components and/or surrogate molecules is greatly facilitated by the application of reaction classes and rate rules. Accurate and versatile rate rules are desirable to improve the predictive accuracy of kinetic models. A major contribution in the literature is the recent work by Bugler et al. (Bugler et al., *J. Phys. Chem. A* 119 (2015) 7510-7527), which has significantly improved rate rules and thermochemical parameters used in kinetic modeling of alkanes. In the present study, it is demonstrated that rate rules can be used

*Corresponding author:

Email address: lcai@itv.rwth-aachen.de (Liming Cai)

1
2
3
4
5
6
7
8
9 and consistently optimized for a set of normal alkanes including *n*-heptane,
10 *n*-octane, *n*-nonane, *n*-decane, and *n*-undecane, thereby improving the pre-
11 dictive accuracy for all the considered fuels. A Bayesian framework is applied
12 in the calibration of the rate rules. The optimized rate rules are subsequently
13 applied to generate a mechanism for *n*-dodecane, which was not part of the
14 training set for the optimized rate rules. The developed mechanism shows
15 accurate predictions compared with published well-validated mechanisms for
16 a wide range of conditions.
17
18

19 *Keywords:*

20 *n*-Alkanes, Rate Rules, Mechanism Development, Optimization and
21 Uncertainty Quantification
22
23

24 **1. Introduction**

25
26
27
28
29
30
31
32
33
34
35
36
37
38
39
40
41
42
43
44
45
46
47
48
49
50
51
52
53
54
55
56
57
58
59
60
61
62
63
64
65
66
67
68
69
70
71
72
73
74
75
76
77
78
79
80
81
82
83
84
85
86
87
88
89
90
91
92
93
94
95
96
97
98
99
100
101
102
103
104
105
106
107
108
109
110
111
112
113
114
115
116
117
118
119
120
121
122
123
124
125
126
127
128
129
130
131
132
133
134
135
136
137
138
139
140
141
142
143
144
145
146
147
148
149
150
151
152
153
154
155
156
157
158
159
160
161
162
163
164
165
166
167
168
169
170
171
172
173
174
175
176
177
178
179
180
181
182
183
184
185
186
187
188
189
190
191
192
193
194
195
196
197
198
199
200
201
202
203
204
205
206
207
208
209
210
211
212
213
214
215
216
217
218
219
220
221
222
223
224
225
226
227
228
229
230
231
232
233
234
235
236
237
238
239
240
241
242
243
244
245
246
247
248
249
250
251
252
253
254
255
256
257
258
259
260
261
262
263
264
265
266
267
268
269
270
271
272
273
274
275
276
277
278
279
280
281
282
283
284
285
286
287
288
289
290
291
292
293
294
295
296
297
298
299
300
301
302
303
304
305
306
307
308
309
310
311
312
313
314
315
316
317
318
319
320
321
322
323
324
325
326
327
328
329
330
331
332
333
334
335
336
337
338
339
340
341
342
343
344
345
346
347
348
349
350
351
352
353
354
355
356
357
358
359
360
361
362
363
364
365
366
367
368
369
370
371
372
373
374
375
376
377
378
379
380
381
382
383
384
385
386
387
388
389
390
391
392
393
394
395
396
397
398
399
400
401
402
403
404
405
406
407
408
409
410
411
412
413
414
415
416
417
418
419
420
421
422
423
424
425
426
427
428
429
430
431
432
433
434
435
436
437
438
439
440
441
442
443
444
445
446
447
448
449
450
451
452
453
454
455
456
457
458
459
460
461
462
463
464
465
466
467
468
469
470
471
472
473
474
475
476
477
478
479
480
481
482
483
484
485
486
487
488
489
490
491
492
493
494
495
496
497
498
499
500
501
502
503
504
505
506
507
508
509
510
511
512
513
514
515
516
517
518
519
520
521
522
523
524
525
526
527
528
529
530
531
532
533
534
535
536
537
538
539
540
541
542
543
544
545
546
547
548
549
550
551
552
553
554
555
556
557
558
559
560
561
562
563
564
565
566
567
568
569
570
571
572
573
574
575
576
577
578
579
580
581
582
583
584
585
586
587
588
589
590
591
592
593
594
595
596
597
598
599
600
601
602
603
604
605
606
607
608
609
610
611
612
613
614
615
616
617
618
619
620
621
622
623
624
625
626
627
628
629
630
631
632
633
634
635
636
637
638
639
640
641
642
643
644
645
646
647
648
649
650
651
652
653
654
655
656
657
658
659
660
661
662
663
664
665
666
667
668
669
670
671
672
673
674
675
676
677
678
679
680
681
682
683
684
685
686
687
688
689
690
691
692
693
694
695
696
697
698
699
700
701
702
703
704
705
706
707
708
709
710
711
712
713
714
715
716
717
718
719
720
721
722
723
724
725
726
727
728
729
730
731
732
733
734
735
736
737
738
739
740
741
742
743
744
745
746
747
748
749
750
751
752
753
754
755
756
757
758
759
760
761
762
763
764
765
766
767
768
769
770
771
772
773
774
775
776
777
778
779
780
781
782
783
784
785
786
787
788
789
790
791
792
793
794
795
796
797
798
799
800
801
802
803
804
805
806
807
808
809
810
811
812
813
814
815
816
817
818
819
820
821
822
823
824
825
826
827
828
829
830
831
832
833
834
835
836
837
838
839
840
841
842
843
844
845
846
847
848
849
850
851
852
853
854
855
856
857
858
859
860
861
862
863
864
865
866
867
868
869
870
871
872
873
874
875
876
877
878
879
880
881
882
883
884
885
886
887
888
889
890
891
892
893
894
895
896
897
898
899
900
901
902
903
904
905
906
907
908
909
910
911
912
913
914
915
916
917
918
919
920
921
922
923
924
925
926
927
928
929
930
931
932
933
934
935
936
937
938
939
940
941
942
943
944
945
946
947
948
949
950
951
952
953
954
955
956
957
958
959
960
961
962
963
964
965
966
967
968
969
970
971
972
973
974
975
976
977
978
979
980
981
982
983
984
985
986
987
988
989
990
991
992
993
994
995
996
997
998
999
1000

Computational fluid dynamic (CFD) calculations of reactive flows have become an important part in the design of combustion devices. A critical factor in performing successful CFD simulations is an adequate representation of fuel chemistry, especially when more complex phenomena are studied, such as auto-ignition, flame stabilization, or pollutant formation. While chemical mechanisms of several species, e. g. methane, ethanol, and *n*-heptane, have been extensively studied in the last few years, the accuracy of the mechanisms for most species requires improvement. Furthermore, there is a growing demand for accurate mechanisms of fuel species that have never been studied. Recently, various new surrogate components, such as *n*-decane [1], *n*-dodecane [2, 3], and 2,5-dimethylhexane [4] have been proposed to improve the performance of surrogate mixtures for petroleum fuels. Moreover, lim-

1
2
3
4
5
6
7
8
9
10
11
12
13
14
15
16
17
18
19
20
21
22
23
24
25
26
27
28
29
30
31
32
33
34
35
36
37
38
39
40
41
42
43
44
45
46
47
48
49
50
51
52
53
54
55
56
57
58
59
60
61
62
63
64
65

ited fossil fuel reserves and a need for renewable energy raise the interest in alternative biofuels. For both kinds of species, mechanisms are generally missing in the literature, which impedes CFD simulations for technical devices burning these fuels. Therefore, the development of accurate chemical reaction schemes becomes even more important, especially for species which have not yet been well studied.

Most chemical mechanisms are still compiled manually [5–11], while several automatic mechanism generation tools have been presented in the literature [12, 13]. The approaches employed in both manual and automatic developments generally rely on the concept of reaction classes and rate rules. In this concept, the fuel specific oxidation steps are described by classes of reactions with the assigned rate constants. Reaction rate constants can be determined from quantum chemistry calculations [14–18] or experimental measurements [19–21]. However, while this is practical and desirable for several very important reactions, it is experimentally and computationally difficult to determine the rate constants of all involved reactions due to their large number. Therefore, for the chemical reactions without rate data from theory or experiment, rate rules are used to specify their rate constant expressions.

Several studies have focused on the development of accurate rate rules. The addition of molecular oxygen to the fuel radicals, which initializes the low temperature oxidation pathway, was studied by Miyoshi [22]. Villano et al. [23, 24] investigated the isomerization rates of alkyl peroxy (RO_2) and peroxy alkylhydroperoxide (O_2QOOH) radicals for C_2 – C_5 alkanes and suggested to use the obtained data also as rate rules for larger hydrocarbon fuels. Due

1
2
3
4
5
6
7
8
9 to their importance, the H-atom migration reactions of RO_2 and O_2QOOH
10 radicals were investigated by Miyoshi [25] and Sharma et al. [26] as well.
11 Also for the decomposition channels of RO_2 and hydroperoxy alkyl (QOOH)
12 radicals, rate rules were determined by Villano et al. [24] and Miyoshi [25].
13 Recently, Bugler et al. [27] evaluated the results [22–26, 28–34] obtained from
14 various levels of quantum theory and then suggested rate rules for the low-
15 temperature oxidation of alkanes. More importantly, the recommended rate
16 rules were provided with their estimated uncertainties [27].
17
18
19
20
21
22
23

24 The knowledge of reaction rate coefficient uncertainties is important, as
25 it can certainly have an impact on prediction accuracy. Uncertainties may
26 come from different sources, for example due to approximations in quantum
27 chemistry calculations or inherent uncertainties in the experimental determi-
28 nation of rate coefficients. While the application of higher levels of quantum
29 theory and the upgrade of measurement facilities may improve the accuracy
30 of rate coefficients, uncertainties still exist. Also the process of parameter
31 optimization depends critically on quantified uncertainties, since modifica-
32 tions to rate coefficients should be made in such a process only within the
33 uncertainty limits.
34
35
36
37
38
39
40
41
42

43 Rate coefficients are often tuned during model development. For this,
44 the important reactions are typically first identified by sensitivity analyses
45 at conditions of interest. Then, the rate parameters for these reactions are
46 modified manually and iteratively within their uncertainty limits to achieve
47 good agreement between model and experiment. In recent years, automatic
48 optimization and uncertainty quantification (UQ) techniques have been suc-
49 cessfully established for improving predictive accuracy of chemical mecha-
50
51
52
53
54
55
56
57
58
59
60
61
62
63
64
65

1
2
3
4
5
6
7
8
9 mechanisms [35–39]. In cases of rate parameter optimizations found in the litera-
10 ture, rate coefficients of elementary reactions are systematically calibrated.
11 However, the rate parameters of most reactions in chemical mechanisms of
12 larger fuels are adapted using rate rules. A large number of reactions could
13 have identical rate parameters, as they are kinetically similar and therefore
14 follow the same rate rule. Obviously, it is not chemically reasonable to tune
15 rate parameters of individual elementary reactions, as this will violate consis-
16 tency of kinetically similar reactions. Recently, Cai and Pitsch [40] proposed
17 an automatic mechanism optimization method based on rate rules. This kind
18 of optimization based on group analysis becomes especially important where
19 the concept of analogy in terms of reaction classes and rate rules is used, e. g.
20 also for the development of polycyclic aromatic hydrocarbon formation and
21 growth chemistry [41].
22
23
24
25
26
27
28
29
30
31
32
33

34 Cai and Pitsch [40] demonstrated the mechanism optimization method
35 based on rate rules by optimizing the model performance of an *n*-pentane
36 mechanism. The method was later applied to calibrate a chemical mechanism
37 for Primary Reference Fuel (PRF) combustion, in which common rate rules
38 were incorporated for *n*-heptane and iso-octane [42]. It was shown that, once
39 the common rate rules were automatically calibrated, both reaction schemes
40 were improved. This indicated the possibility to develop optimized universal
41 rate rules, with which accurate chemical mechanisms can be derived for a set
42 of fuels rather than for only one particular fuel.
43
44
45
46
47
48
49
50

51 An additional aspect of optimization and uncertainty quantification is to
52 extract useful information from available data. Typically, experimental data
53 sets are required for model validation. However, despite the increasing inter-
54
55
56
57
58
59
60
61
62
63
64
65

1
2
3
4
5
6
7
8
9 est in long chain fuel species, limited measurements have been performed for
10 them in the literature. The lack of information makes it difficult to derive ac-
11 curate mechanisms for these fuels of interest. An uncertainty quantification
12 framework gains information from the available measurements for shorter fu-
13 els to update the knowledge about rate rules. Once these constrained rate
14 rules are used to construct chemical models of longer chain fuels, the derived
15 models inherit the information from the shorter ones. This creates confi-
16 dence in the prediction accuracy of mechanisms that cannot be extensively
17 validated due to the lack of experimental measurements.

18
19 In this study, it is demonstrated that rate rules calibrated automatically
20 for a number of smaller fuels can be applied in the model development of
21 similar but larger hydrocarbons, yielding predictions that are improved com-
22 pared to published mechanisms for the same fuel. For this purpose, the rate
23 rules for normal alkanes are studied here. A training of the rate rules is
24 first performed, where the rate rules for *n*-alkanes are optimized against a
25 large experimental database for *n*-heptane, *n*-octane, *n*-nonane, *n*-decane,
26 and *n*-undecane using a Bayesian framework. As a test case, the optimized
27 rate rules are subsequently employed to derive a chemical mechanism for
28 *n*-dodecane. The derived *n*-dodecane mechanism is then compared with ex-
29 perimental measurements, a published well-validated mechanism [43], and
30 a mechanism developed with rate rules previously provided in the litera-
31 ture [8, 27]. The validity of the optimized rate rules is thus examined, and
32 the predictive quality of the application of the optimized rate rules in the
33 development of chemical mechanisms for different fuels is demonstrated.

34
35 The presentation of this paper is organized as follows. First, the op-
36
37
38
39
40
41
42
43
44
45
46
47
48
49
50
51
52
53
54
55
56
57
58
59
60
61
62
63
64
65

1
2
3
4
5
6
7
8
9 timization methodology based on rate rules is briefly introduced. Next, a
10 mechanism for C₇-C₁₁ normal alkanes is developed with the up-to-date ki-
11 netic knowledge. Following this, the automatic calibration of the applied rate
12 rules is performed. The article closes with the validation of the *n*-dodecane
13 mechanism developed based on the optimized rate rules.
14
15
16
17
18
19

20 **2. Methodology**

21
22
23 Recently, Cai and Pitsch [40] extended the methods by Sheen and Wang [37]
24 and Frenklach [35] for automatic calibration of chemical kinetic models by
25 performing optimization of reaction rate rules. The methodology leads to a
26 chemically more consistent model calibration and improves the model pre-
27 diction accuracy significantly. As it categorizes chemically similar reactions
28 into one calibration objective, the number of uncertain parameters decreases.
29 This strongly reduces the computational effort of the optimization process
30 and therefore enables optimization of low temperature auto-ignition, where
31 many chemical reactions appear as important. The method was first applied
32 to calibrate an *n*-pentane mechanism [40] and afterwards employed to im-
33 prove a chemical mechanism for *n*-heptane and iso-octane mixtures, in which
34 common rate rules are incorporated for both fuels [42]. Once the common
35 rate rules are calibrated, both reaction schemes for *n*-heptane and iso-octane
36 are optimized. As the number of rate rules does not increase with the number
37 of fuels in the mechanism, the computational advantage is further advanced.
38
39
40
41
42
43
44
45
46
47
48
49
50
51
52 The methodology is described briefly in this section.
53
54
55
56
57
58
59
60
61
62
63
64
65

1
2
3
4
5
6
7
8
9 *2.1. Reaction classes and rate rules*

10
11 In the present model development process, the fuel specific chemistry of
12 large hydrocarbon fuels is developed based on the approach of using reaction
13 classes and rate rules. Many reaction mechanisms have been built recently in
14 this manner for fuels of interest [5–11]. For these developments, 30 reaction
15 classes, listed in the Supplementary material, were used to derive the chemical
16 mechanisms [8].
17
18
19
20
21

22
23 Rate rules are employed in this approach to specify the rate constant
24 expressions for the individual elementary reactions provided by the reaction
25 classes. The rate rules for the individual classes were determined based on
26 available chemical kinetic knowledge [5, 8]. If the reactions in a class are
27 carbon site specific or their strain energy barriers are sensitive to the size of
28 transition state rings, several rate rules can be found within this class (e.g.
29 Class 15: $\text{RO}_2 = \text{QOOH}$). For reaction classes with limited information of
30 similar reaction types (e.g. Class 16: $\text{RO}_2 = \text{alkene} + \text{HO}_2$), only one
31 rate rule is employed. In the optimization method proposed by Cai and
32 Pitsch [40], each rate rule is supposed to be a potential active parameter of
33 the model calibration. Once a rate rule is calibrated, the rate constants of
34 all reactions using this rule are consistently modified.
35
36
37
38
39
40
41
42
43
44
45

46
47 *2.2. Optimization algorithm*

48
49 In previous studies [40, 42], the method of uncertainty minimization using
50 polynomial chaos expansion (MUM-PCE) proposed by Sheen and Wang [37]
51 has been successfully used to calibrate the rate rules and to estimate their
52 uncertainties. MUM-PCE estimates posterior probability density functions
53 (PDFs) of parameters by assuming that these PDFs are either normally or
54
55
56
57
58

1
2
3
4
5
6
7
8
9 uniformly distributed [37]. The means of the optimized parameters are de-
10 termined based on the optimization approach developed originally by Fren-
11 klach [35], and the covariance matrix is then estimated analytically. MUM-
12 PCE can be seen as a simplified form of the Bayesian approach for uncertainty
13 quantification, which is exempted from the assumption of a particular form
14 for posterior PDFs. In this study, instead of MUM-PCE, the Bayesian ap-
15 proach is applied to optimize the rate rules, to quantify their uncertainties,
16 and to minimize the model uncertainties.
17
18
19
20
21
22
23
24

25 *2.2.1. Bayesian approach*

26
27 The Bayes' theorem provides a probabilistic approach to gain information
28 about model parameters from given experimental data. In many cases, the
29 exact values of model quantities are unknown, but some information about
30 these parameters has been gained already. Within the Bayesian interpreta-
31 tion, model parameters are treated as random variables and therefore, the
32 state of knowledge about the parameter values can be represented by the PDF
33 of the random variables. The knowledge of these parameters in terms of joint
34 PDFs can be updated with new data according to Bayes' theorem [44, 45].
35
36
37
38
39
40
41
42

43 In probability theory and statistics, the Bayes' theorem [44, 45] states for
44 the given quantities a and b that
45

$$46 \quad p(a|b) = \frac{p(a)p(b|a)}{p(b)} \quad , \quad (1)$$

47
48 where $p(a)$ and $p(b)$ are the probability distributions of a and b , respectively.
49
50
51
52
53
54
55
56
57
58
59
60
61
62
63
64
65
66
67
68
69
70
71
72
73
74
75
76
77
78
79
80
81
82
83
84
85
86
87
88
89
90
91
92
93
94
95
96
97
98
99
100
101
102
103
104
105
106
107
108
109
110
111
112
113
114
115
116
117
118
119
120
121
122
123
124
125
126
127
128
129
130
131
132
133
134
135
136
137
138
139
140
141
142
143
144
145
146
147
148
149
150
151
152
153
154
155
156
157
158
159
160
161
162
163
164
165
166
167
168
169
170
171
172
173
174
175
176
177
178
179
180
181
182
183
184
185
186
187
188
189
190
191
192
193
194
195
196
197
198
199
200
201
202
203
204
205
206
207
208
209
210
211
212
213
214
215
216
217
218
219
220
221
222
223
224
225
226
227
228
229
230
231
232
233
234
235
236
237
238
239
240
241
242
243
244
245
246
247
248
249
250
251
252
253
254
255
256
257
258
259
260
261
262
263
264
265
266
267
268
269
270
271
272
273
274
275
276
277
278
279
280
281
282
283
284
285
286
287
288
289
290
291
292
293
294
295
296
297
298
299
300
301
302
303
304
305
306
307
308
309
310
311
312
313
314
315
316
317
318
319
320
321
322
323
324
325
326
327
328
329
330
331
332
333
334
335
336
337
338
339
340
341
342
343
344
345
346
347
348
349
350
351
352
353
354
355
356
357
358
359
360
361
362
363
364
365
366
367
368
369
370
371
372
373
374
375
376
377
378
379
380
381
382
383
384
385
386
387
388
389
390
391
392
393
394
395
396
397
398
399
400
401
402
403
404
405
406
407
408
409
410
411
412
413
414
415
416
417
418
419
420
421
422
423
424
425
426
427
428
429
430
431
432
433
434
435
436
437
438
439
440
441
442
443
444
445
446
447
448
449
450
451
452
453
454
455
456
457
458
459
460
461
462
463
464
465
466
467
468
469
470
471
472
473
474
475
476
477
478
479
480
481
482
483
484
485
486
487
488
489
490
491
492
493
494
495
496
497
498
499
500
501
502
503
504
505
506
507
508
509
510
511
512
513
514
515
516
517
518
519
520
521
522
523
524
525
526
527
528
529
530
531
532
533
534
535
536
537
538
539
540
541
542
543
544
545
546
547
548
549
550
551
552
553
554
555
556
557
558
559
560
561
562
563
564
565
566
567
568
569
570
571
572
573
574
575
576
577
578
579
580
581
582
583
584
585
586
587
588
589
590
591
592
593
594
595
596
597
598
599
600
601
602
603
604
605
606
607
608
609
610
611
612
613
614
615
616
617
618
619
620
621
622
623
624
625
626
627
628
629
630
631
632
633
634
635
636
637
638
639
640
641
642
643
644
645
646
647
648
649
650
651
652
653
654
655
656
657
658
659
660
661
662
663
664
665
666
667
668
669
670
671
672
673
674
675
676
677
678
679
680
681
682
683
684
685
686
687
688
689
690
691
692
693
694
695
696
697
698
699
700
701
702
703
704
705
706
707
708
709
710
711
712
713
714
715
716
717
718
719
720
721
722
723
724
725
726
727
728
729
730
731
732
733
734
735
736
737
738
739
740
741
742
743
744
745
746
747
748
749
750
751
752
753
754
755
756
757
758
759
760
761
762
763
764
765
766
767
768
769
770
771
772
773
774
775
776
777
778
779
780
781
782
783
784
785
786
787
788
789
790
791
792
793
794
795
796
797
798
799
800
801
802
803
804
805
806
807
808
809
810
811
812
813
814
815
816
817
818
819
820
821
822
823
824
825
826
827
828
829
830
831
832
833
834
835
836
837
838
839
840
841
842
843
844
845
846
847
848
849
850
851
852
853
854
855
856
857
858
859
860
861
862
863
864
865
866
867
868
869
870
871
872
873
874
875
876
877
878
879
880
881
882
883
884
885
886
887
888
889
890
891
892
893
894
895
896
897
898
899
900
901
902
903
904
905
906
907
908
909
910
911
912
913
914
915
916
917
918
919
920
921
922
923
924
925
926
927
928
929
930
931
932
933
934
935
936
937
938
939
940
941
942
943
944
945
946
947
948
949
950
951
952
953
954
955
956
957
958
959
960
961
962
963
964
965
966
967
968
969
970
971
972
973
974
975
976
977
978
979
980
981
982
983
984
985
986
987
988
989
990
991
992
993
994
995
996
997
998
999
1000

1
2
3
4
5
6
7
8
9 implies that

$$p_{\text{post}}(x|\eta^{\text{obs}}) = \frac{p_{\text{prior}}(x)\pi(x;\eta^{\text{obs}})}{\int p_{\text{prior}}(x)\pi(x;\eta^{\text{obs}})dx} . \quad (2)$$

10
11 Here, p_{prior} is the prior PDF, which quantifies available information about
12 the parameters x . While this information may incorporate knowledge from
13 previously performed experiments, it is independent of the current experi-
14 mental data set η^{obs} . In the literature, uniform and Gaussian-shaped PDF
15 forms are most commonly used as priors [46]. A uniform prior assigns a con-
16 stant probability density to the parameter values within given boundaries,
17 while a Gaussian prior assigns higher density near the mean. p_{post} denotes
18 the posterior PDF, which quantifies the parameter knowledge after incor-
19 porating the information from the experimental data η^{obs} . The likelihood
20 function $\pi(x;\eta^{\text{obs}})$ quantifies the agreement between the model and the data
21 for specific values of the parameters:
22
23
24
25
26
27
28
29
30
31
32
33
34
35

$$\pi(x;\eta^{\text{obs}}) = p_{\text{like}}(\eta|x)|_{\eta=\eta^{\text{obs}}} . \quad (3)$$

36
37 In Eq. (3), η is the model prediction. Due to inadequacies in the model
38 (model error) and due to inadequacies in the measurement process (exper-
39 imental error), the model predictions differ from the observed values. The
40 PDF p_{like} represents the state of knowledge regarding these errors. When
41 p_{like} is evaluated at the observed values η^{obs} and considered as a function of
42 the model parameters x , it becomes the likelihood function $\pi(x;\eta^{\text{obs}})$ [46].
43 In order to construct a likelihood function, an error model should be defined
44 first. Here, the error model is defined as:
45
46
47
48
49
50
51
52
53
54
55
56
57
58
59
60
61
62
63
64
65

$$\eta_i^{\text{obs}} = \eta_i(x) + \epsilon_i , \quad (4)$$

1
 2
 3
 4
 5
 6
 7
 8
 9 where ϵ_i refers to the experimental error of the measurement i , consequently
 10 assuming an exact model. Unlike several studies in the past [46, 47], the use
 11 of a hyper-parameter to identify model errors past is not used here. Since
 12 the focus here is on the development of a calibrated chemical mechanism for
 13 use in a deterministic manner, such a model-error approach [46, 47] is not
 14 suitable. If data can be obtained with zero errors, the assumption states that
 15 the parameters could be fitted perfectly and the model could thus predict
 16 experiment exactly. The errors in experiments are assumed to be indepen-
 17 dent, normally distributed random variables with $\epsilon_i \sim \mathcal{N}_i(0, \sigma_i^2)$. Thus, the
 18 likelihood function with n experiments can be formulated as:
 19
 20
 21
 22
 23
 24
 25
 26
 27

$$28 \pi(x; \eta^{\text{obs}}) = \frac{1}{\prod_{i=1}^n (2\pi\sigma_i^2)^{\frac{1}{2}}} \exp \left[-\frac{1}{2} \sum_{i=1}^n \frac{1}{\sigma_i^2} (\eta_i^{\text{obs}} - \eta_i(x))^2 \right]. \quad (5)$$

29
 30
 31
 32
 33 As mentioned by Braman et al. [46], the Bayesian approach provides a natu-
 34 rally self-consistent process for learning based on available information. The
 35 posteriors from one optimization can be further used as the priors for subse-
 36 quent calibrations, once more experimental measurements become available.
 37
 38
 39
 40
 41

42 2.2.2. Computational details

43
 44 In the present study, the Bayesian approach is implemented with the
 45 statistical QUESO library [48]. For each experimental condition included in
 46 the optimization process, a sensitivity analysis of the rate rules is carried
 47 out. The rate rules with the highest sensitivities ($>2\%$) in the range of the
 48 experimental conditions are selected automatically as active parameters. The
 49 uncertainties of the rate rules are assumed to be temperature-independent
 50 according to Ref. [27], and thus only the Arrhenius pre-exponential factors
 51
 52
 53
 54
 55
 56
 57
 58
 59
 60
 61
 62
 63
 64
 65

1
2
3
4
5
6
7
8
9 A are considered as calibration objectives. The current state of knowledge
10 about the rate rules is represented by uniformly distributed PDFs bounded
11 by the lower and upper limits of the pre-exponential factors. The prior
12 pre-exponential factors and their uncertainty limits used here are shown in
13 Table 2. Note that the prior selection affects the posterior distributions,
14 as quantified in Ref. [46]. While the bounds of the uniform prior limit the
15 posterior distribution, the Gaussian prior does not posit a bound on the
16 parameter [46], which is useful if this parameter information is not available
17 a priori. However, for an underconstrained calibration case, the application
18 of Gaussian priors can shift the posteriors to a domain, which is not covered
19 by the existing rate data.
20
21
22
23
24
25
26
27
28
29

30 The likelihood function is specified according to Eq. (5). The poste-
31 rior PDFs are estimated by solving Eq. (2) with the Markov Chain Monte
32 Carlo (MCMC) sampling algorithm [46, 49, 50]. In the present study, the
33 mean values of the posterior PDFs are defined as the pre-exponential fac-
34 tors of the optimized rate rules and further incorporated in chemical mech-
35 anisms. It is also found that the performance of the mechanism developed
36 with the mean values of the posterior PDFs is almost identical with the
37 one based on the peak values of PDFs. Due to the large number of sam-
38 ples, the model predictions are calculated through the response surface tech-
39 nique [35], which relates the model parameters to the prediction targets in
40 form of a second order polynomial. The coefficients in the response surface
41 are calculated by the sensitivity analysis based (SAB) method [51], and the
42 required simulations are performed using the appropriate reactor modules in
43 the FlameMaster [52] code, with the source code available at www.itv.rwth-
44
45
46
47
48
49
50
51
52
53
54
55
56
57
58
59
60
61
62
63
64
65

1
2
3
4
5
6
7
8
9 aachen.de/downloads/flamemaster/.

10 11 12 **3. Mechanism development** 13 14

15 A newly developed kinetic mechanism for C₇–C₁₁ normal alkanes is pre-
16 sented in this section. The chemical mechanism for *n*-alkanes and 2-methylalkanes [8]
17 served as the starting point in the development procedure. This mecha-
18 nism [8] was updated according to the recent work by Bugler et al. [27].
19 Subsequently, the mechanism was reduced to a skeletal level in order to en-
20 able the optimization within a reasonable computational time.
21
22
23
24
25
26

27 *3.1. Mechanism modification* 28

29 Sarathy et al. [8] presented a detailed chemical kinetic mechanism (re-
30 ferred to as “LLNL” mechanism) for the oxidation of singly methylated iso-
31 alkanes (i.e., 2-methylalkanes) ranging from C₇–C₂₀, which also included an
32 updated version of the previously published model for C₈–C₁₆ *n*-alkanes [7].
33 While the model predicted the oxidation of normal alkanes with a moderate
34 accuracy, discrepancies were observed between experiments and simulations,
35 especially for ignition delay times [8]. Recently, Bugler et al. [27] investi-
36 gated the auto-ignition of three pentane isomers and improved the general
37 understanding of low temperature oxidation kinetics. They stated that errors
38 from both thermochemistry and rate constant assignments compensated each
39 other in past models [5–7]. Based on a thorough literature review, they re-
40 visited rate rules for important low temperature reaction classes. Species ther-
41 mochemical data were estimated with refined group additivity values from
42 Burke et al. [53]. Moreover, alternative isomerization pathways of O₂QOOH
43 radicals were proposed. In contrast to the conventional isomerization, in
44
45
46
47
48
49
50
51
52
53
54
55
56
57
58

1
2
3
4
5
6
7
8
9 which an H atom is abstracted from the carbon site bonded to the hydroperoxy
10 group, the H atom can now also be released from a normal C-H bond
11 via 5, 6, 7, and 8-membered transition state rings. Due to the lower energy
12 barriers, the channels with six-membered transition state rings are dominant.
13 All these modifications [27] were incorporated into the LLNL mechanism in
14 this study.
15
16
17
18
19

20 The update was performed in three steps: (a) The thermochemical data
21 of species involved in the oxidation of C₇–C₁₁ alkanes were first recalculated
22 using the group additivity method [54] with the revised group values [53]
23 in the THERM code [55]. (b) Following this, the rate rules in the LLNL
24 mechanism were replaced by the rate rules recommended in Ref. [27]. For
25 H-atom abstractions from the fuel by OH radicals, Sivaramakrishnan and
26 Michael [56] reported different barrier heights at various carbon sites and
27 experimentally investigated the site specific rate rules for these reactions in a
28 rigorous manner. These accurate site specific rate rules [56] were also incor-
29 porated into the mechanism. (c) Finally, the alternative reaction pathways of
30 O₂QOOH producing di-hydroperoxy alkyl radicals P(OOH)₂ were included in
31 the mechanism. Only the channels with six-membered transition state rings
32 were taken into account due to their lower energy barriers and expected dom-
33 inance [27]. Two consumption channels were proposed for P(OOH)₂ radicals.
34 The P(OOH)₂ radical can either go through a β -scission to form an olefin
35 and a hydroperoxyl radical or decomposes to produce a cyclic ether and an
36 OH radical. The cyclization of P(OOH)₂ radicals takes place at O₂QOOH to
37 P(OOH)₂ isomerization site. For the O₂QOOH species having conventional
38 ketohydroperoxide formation pathways via 6-membered transition state ring,
39
40
41
42
43
44
45
46
47
48
49
50
51
52
53
54
55
56
57
58
59
60
61
62
63
64
65

1
2
3
4
5
6
7
8
9 alternative pathways were not considered in the mechanism. The modified
10 mechanism consists of 1692 species among 11015 reactions (forward and back-
11 ward counted separately). The effects of these revisions are demonstrated in
12 the following example in terms of the ignition delay times of *n*-decane.
13
14

15
16
17 Figure 1 contains the ignition delay times of stoichiometric *n*-decane/air
18 mixtures at 12 atm. Over the entire temperature range, the LLNL model [8]
19 predicts the ignition delay times with decent accuracy. At intermediate tem-
20 peratures, it underpredicts the data with a factor of around 3. After the
21 revision of the thermochemistry, the computed ignition delays increase sig-
22 nificantly at intermediate temperatures. With the further update of the rate
23 rules, the numerical results decrease in the low to intermediate temperature
24 range. Compared with these two alterations, the impact of alternative path-
25 ways of O₂QOOH radicals on ignition is smaller but not negligible. Normally,
26 an O₂QOOH radical undergoes an internal H-atom migration to release an
27 OH radical and forms a ketohydroperoxide. The ketohydroperoxide decom-
28 poses to produce a second OH radical, which results in a chain branching
29 in the low temperature range. Alternatively, the O₂QOOH radical can now
30 isomerize to form a di-hydroperoxy alkyl radical. While this isomerization
31 step does not directly release an OH radical, the consumption pathways of
32 P(OOH)₂ can produce two OH radicals. Again, a chain branching path-
33 way is established at low temperatures. Compared with the conventional
34 isomerization via five- or eight-membered transition state rings, the alterna-
35 tive channel is based on a rapid six-membered ring H-atom migration and
36 thus becomes favorable. As shown in Fig. 1, this alternative isomerization
37 enhances the fuel ignition propensity at low to intermediate temperatures.
38
39
40
41
42
43
44
45
46
47
48
49
50
51
52
53
54
55
56
57
58
59
60
61
62
63
64
65

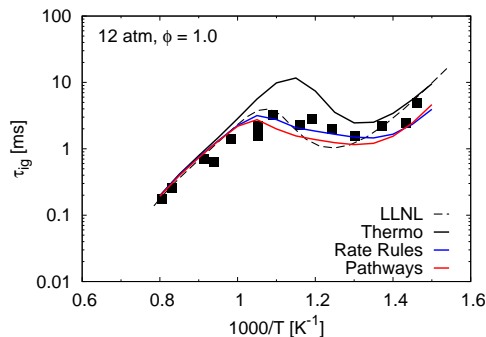


Figure 1: Ignition delay times of *n*-decane/air mixtures. Symbols denote experimental measurements [58]. Dashed line shows the results using the LLNL model [8]. Black, blue, and red solid lines show the results for the model after revision steps (a), (b), and (c), respectively.

The effects of these three modifications on the auto-ignition of *n*-decane are consistent with those reported for pentane isomers [27] and those observed for the other normal alkanes studied in this work. The cases of *n*-octane and *n*-nonane are shown in the Supplementary material. In comparison with the previous LLNL mechanism, the modified mechanism predicts the ignition delay times at low and intermediate temperatures with slightly improved accuracy. The slope of the measured ignition delay times in the intermediate temperature range is well reproduced by the updated mechanism. The developed kinetic knowledge from Bugler et al. [27] demonstrates here the capability to improve the model prediction precision. Nevertheless, differences still exist between the updated mechanism and the experimental data, which motivates the further calibration of rate rules.

3.2. Mechanism reduction

While the application of the response surface technique [35, 51] contributes to a significant reduction in the computational cost of Bayesian analysis, a large amount of numerical calculations are still required to generate the response surface. In order to minimize this computational effort, the updated mechanism was reduced to a skeletal level using a multi-stage reduction strategy proposed by Pepiot-Desjardins and Pitsch [57]. The directed relation graph method with error propagation (DRGEP) [57] selects the important reaction channels based on the evaluation of species production and consumption rates. The reduction procedure involved the elimination of species and reactions. The lumping of chemical species presented in Ref. [57] was excluded, as the isomerization of intermediates plays a major role in fuel oxidation and thus the involved rate coefficients are of particular importance for model predictions. The targets in the reduction include concentrations of various major species for varying initial pressures, temperatures, and equivalence ratios. Very small error tolerances were specified for the deviations of targets between the skeletal and the detailed mechanisms. This reduction process, and specifically the error propagation algorithm, ensure that only those species and reactions are removed, which have a minimal impact on the chemistry of the reduction targets. Ignition delay times are not direct targets in the reduction, but are inherently preserved by correctly predicting the chemistry of the target species. The reduced model is composed of 624 species with 2727 reactions (forward and backward counted separately). The computed ignition delay times of *n*-decane using the detailed and the reduced mechanisms are compared in Fig. 2. For the experimental conditions

1
2
3
4
5
6
7
8
9
10
11
12
13
14
15
16
17
18
19
20
21
22
23
24
25
26
27
28
29
30
31
32
33
34
35
36
37
38
39
40
41
42
43
44
45
46
47
48
49
50
51
52
53
54
55
56
57
58
59
60
61
62
63
64
65

studied, the differences between the detailed and the reduced mechanisms are marginal. Good agreement between both mechanisms is also observed for the auto-ignition of *n*-heptane, *n*-octane, *n*-nonane, and *n*-undecane.

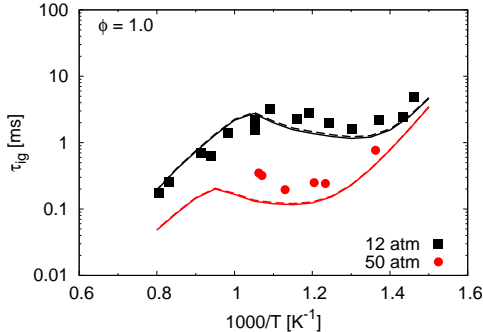


Figure 2: Ignition delay times of *n*-decane/air mixtures. Symbols denote experimental measurements [58]. Solid lines show the results for the model developed in Section 3.1, and dashed lines show the results for the reduced model.

4. Rate rule calibration

In this section, the training of the rate rules is described. A large number of experimental data sets for *n*-heptane, *n*-octane, *n*-nonane, *n*-decane, and *n*-undecane were taken into consideration. Using the Bayesian method described in Section 2, the rate rules used in the reduced chemical mechanism for C₇–C₁₁ *n*-alkanes were calibrated automatically for the given data sets for different fuels.

4.1. Experimental database

An overview of the experimental data sets used in the Bayesian analysis is shown in Table 1. Experimental ignition delay times were reported

1
2
3
4
5
6
7
8
9 for *n*-heptane [59, 60], *n*-octane [8], and *n*-decane [58, 61] for a variety of
10 conditions covering the entire range of temperatures. For *n*-nonane and
11 *n*-undecane, measurements were solely performed for diluted mixtures at high
12 temperatures [62, 63]. Overall, 198 experimental data points were taken into
13 account in the optimization process.
14
15
16
17

18
19 Campbell et al. [59] stated an uncertainty of $\pm 25\%$ for their *n*-heptane
20 ignition data. The uncertainties in the ignition delay times were mainly at-
21 tributed to uncertainties in reflected shock pressures and temperatures, mix-
22 ture compositions, and signal determinations [59]. An uncertainty of $\pm 10\%$
23 was estimated by Rotavera and Petersen [62] for the ignition delay times of
24 *n*-nonane and *n*-undecane. A pressure uncertainty of ± 2 bar was reported in
25 Ref. [60] for the auto-ignition of *n*-heptane/air mixtures at a pressure of 40
26 bar. This pressure variation was related to a standard deviation of approxi-
27 mately 10% in ignition delays. These reported uncertainties [59, 60, 62] were
28 used in the calibration for the corresponding experiments. Uncertainty esti-
29 mates were missing in several studies [8, 58, 61]. For these measurements,
30 an uncertainty of $\pm 10\%$ was assumed. Pressure increase due to shock at-
31 tenuation was observed in the shock tube measurements by Rotavera and
32 Petersen [62] and Sarathy et al. [8]. It was found [8] that the effect of pres-
33 sure increase becomes important only at very low temperatures. Therefore,
34 the measurements for *n*-octane [8] at very low temperatures were excluded
35 from the optimization.
36
37
38
39
40
41
42
43
44
45
46
47
48
49
50

51 The database excludes the ignition delay times from rapid compression
52 machines (RCM), as common 0D RCM simulation approaches utilizing pres-
53 sure traces of non-reactive mixtures are associated with a maximum predic-
54
55
56
57
58
59
60
61
62
63
64
65

1
2
3
4
5
6
7
8
9 tion deviation of 30% [68]. The experimental burning velocities of C₇–C₁₁
10 alkanes were included in the calibration process. However, these targets were
11 automatically exempted from the optimization after sensitivity analyses, as
12 their prediction are found to be negligibly influenced by the rate rules. The
13 prediction of flame speeds depends solely on the reactions involved in the base
14 mechanism [10]. Also, the prediction of small hydrocarbon species profiles
15 typically measured in flow and jet stirred reactors is highly sensitive to the re-
16 actions involving small species [43, 69]. Therefore, this study focuses on fuel
17 auto-ignition in shock tubes, which is mainly influenced by the fuel specific
18 reactions and can be accurately reproduced by common 0D simulations.

19
20
21
22
23
24
25
26
27
28 Note that two data sets were reported by Campbell et al. [59] for *n*-
29 heptane at identical conditions. The first data set was measured in a con-
30 ventional shock tube, where the auto-ignition takes place nominally at a
31 constant volume. The second set was measured with the novel Constrained
32 Reaction Volume (CRV) technique under constant pressure conditions. It
33 was found in this study that the experimental data set measured with the
34 novel CRV technique was inconsistent with other experimental data. There-
35 fore, this data set was excluded from the automatic calibration. A more
36 detailed discussion is presented in Section 4.4.

37 38 39 40 41 42 43 44 45 46 *4.2. Model calibration and uncertainty quantification*

47
48
49 The reduced mechanism for the oxidation of C₇–C₁₁ normal alkanes was
50 subjected to the automatic optimization. The sensitive rate rules were chosen
51 as active parameters. For the given experimental data sets, the joint posterior
52 PDFs of the rate rules were determined based on the Bayesian theorem. By
53 means of a Monte Carlo sampling algorithm, the uncertainties of the rate
54
55
56
57
58

Fuel	Pressure [bar]	Equivalence Ratio [-]	No. Data	Ref.
<i>n</i> -Heptane	6.5	0.75 (diluted)	22	[59]
	13.5	0.5, 1.0, 2.0	49	[60]
	42.0	0.5, 1.0, 2.0	22	[60]
<i>n</i> -Octane	20.3	0.5, 1.0, 1.5	59	[8]
<i>n</i> -Nonane	1.5	1.0 (diluted)	10	[62, 63]
	12.2	1.0	14	[58]
<i>n</i> -Decane	50.7	1.0	6	[58]
	81.1	0.5, 1.0	10	[61]
<i>n</i> -Undecane	1.5	1.0 (diluted)	6	[62]

Table 1: Experimental database.

rules were propagated into the simulation results. In this way, the model prediction uncertainties were quantified.

The ignition delay times computed with the optimized mechanism for normal alkanes are presented in Figs. 3–7 in comparison with measurements. It is shown that the model with the optimized common rate rules yields a very good agreement with experiments. Compared with the mechanism developed in Section 3, which incorporates the up-to-date kinetic knowledge, the optimized model predicts the ignition delay times with improved accuracy over a wide variety of initial conditions, especially at intermediate temperatures.

Note that ignition delay times are generally underpredicted by the un-optimized model in the low and intermediate temperature ranges. A strong deviation is seen for the case of *n*-heptane, which indicates that the un-optimized set of rate rules is less suitable for this fuel, while relatively more

appropriate for larger species. In addition, the prior set predicts lean auto-ignition with higher accuracy than auto-ignition at rich conditions. These observations lend further support to the proposed methodology, which calibrates rate rules across a family of fuels rather than for each fuel individually and includes a large number of experimental data covering a wide range of initial conditions.

The optimized model is validated in the Supplementary material against the species concentration measurements for *n*-heptane in **jet stirred reactors** [64, 65] and for *n*-octane [66] and *n*-decane [67] in flow reactors, which were not part of the optimization. Nevertheless, the model again appears satisfactory.

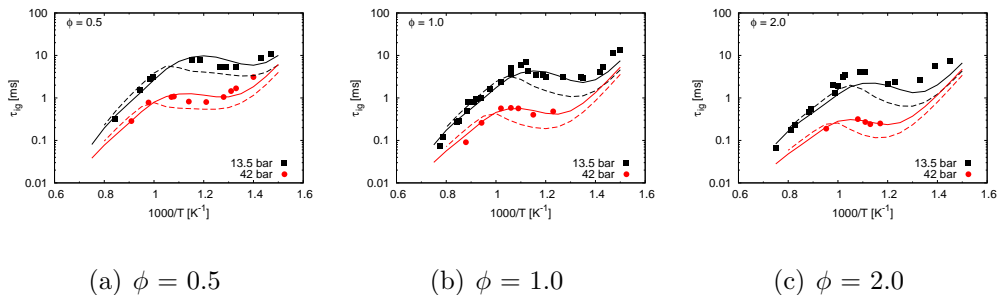


Figure 3: Ignition delay times of *n*-heptane/air mixtures. Symbols denote experimental measurements [60]. Solid lines show the numerical results for the present optimized model, and dashed lines show the results for the unoptimized model.

4.3. Rate rules

57 important rate rules from 21 reaction classes were calibrated automatically. The sensitive reaction classes at high temperatures contain the fuel decomposition (C1), the H-abstraction from fuel (C2), the decomposition (C3) and the isomerization (C4) of fuel radicals, and the decomposition of

1
2
3
4
5
6
7
8
9
10
11
12
13
14
15
16
17
18
19
20
21
22
23
24
25
26
27
28
29
30
31
32
33
34
35
36
37
38
39
40
41
42
43
44
45
46
47
48
49
50
51
52
53
54
55
56
57
58
59
60
61
62
63
64
65

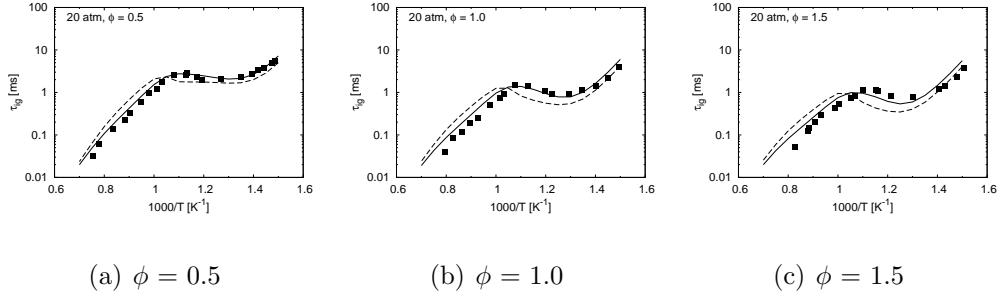


Figure 4: Ignition delay times of *n*-octane/air mixtures. Symbols denote experimental measurements [8]. Solid lines show the numerical results for the present optimized model, and dashed lines show the results for the unoptimized model.

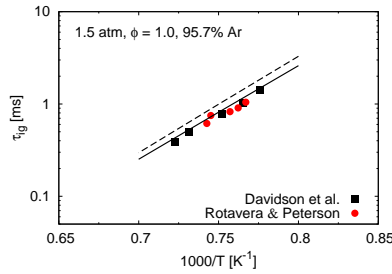


Figure 5: Ignition delay times of *n*-nonane/oxygen/argon mixtures. Symbols denote experimental measurements [62, 63]. Solid line shows the numerical results for the present optimized model, and dashed line shows the results for the unoptimized model.

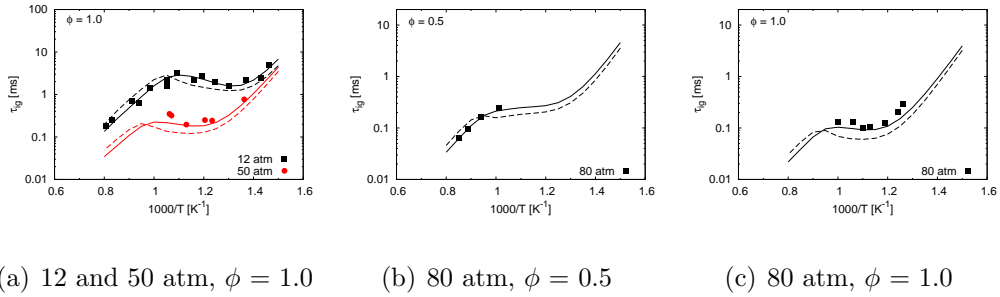


Figure 6: Ignition delay times of *n*-decane/air mixtures. Symbols denote experimental measurements [58, 61]. Solid lines show the numerical results for the present optimized model, and dashed lines show the results for the unoptimized model.

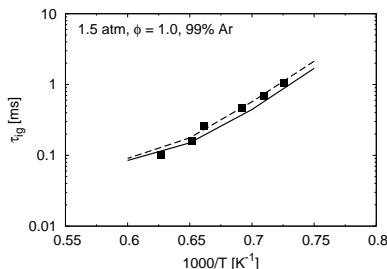


Figure 7: Ignition delay times of *n*-undecane/oxygen/argon mixtures. Symbols denote experimental measurements by Rotavera and Petersen [62]. Solid line shows the numerical results for the present optimized model, and dashed line shows the results for the unoptimized model.

alkenyl radicals (C8) as well as alkene species (C9). The reaction classes 11, 15, 26, 27, and 28 complete the low temperature chain branching pathway and are dominant at low to intermediate temperatures. Several additional reaction classes are also rate-controlling at low to intermediate temperatures. In reaction class 13, alkyl radicals react with HO₂ to yield an OH, leading to chain propagation. The concerted elimination of RO₂ radicals occurs via 5-membered transition state rings. Besides the oxidation pathway, three decomposition channels of QOOH radicals (C23, C24, and C25) also play a major role at relevant conditions. All these reaction steps compete with the chain branching pathway and thus prolong auto-ignition. The alternative isomerization of O₂QOOH is found to be sensitive as well. The promoting effect of this reaction class on ignition was shown in Section 3. Note that only the rate rules for primary and secondary carbon sites are considered in the present work, as *n*-alkanes do not contain tertiary carbon sites.

The calibrated rate rules are summarized in Table 2 along with the orig-

1
2
3
4
5
6
7
8
9
10
11
12
13
14
15
16
17
18
19
20
21
22
23
24
25
26
27
28
29
30
31
32
33
34
35
36
37
38
39
40
41
42
43
44
45
46
47
48
49
50
51
52
53
54
55
56
57
58
59
60
61
62
63
64
65

inal values and their uncertainties. Uncertainty limits were reported for several low temperature reaction classes (e. g. Class 23: QOOH = cyclic + OH) by Bugler et al. [27] and were taken into account in this work. The site specific rate rules for the H-abstraction from the fuel by OH radical proposed by Sivaramakrishnan and Michael [56] predict the total rate constant for *n*-heptane + OH within an uncertainty of 10%. This corresponds to an uncertainty estimate of 41.9% for the rate rule at the P₁ carbon site at a temperature of 1000 K, if the error in the overall rate is caused exclusively by this rate rule. Similarly, uncertainties of the rate rules at S₀₁, S₁₁, and S_{11'} sites are deduced as 29.1%, 39.4%, and 60.8%, respectively. For the rate rules without uncertainty estimates in the literature, an uncertainty factor of four is defined, as large uncertainties can be expected [40].

It is found that most rate rules are altered strongly after the calibration. One reason for this is the form of the prior PDF of the rate rule values. A uniform distribution indicates a minor confidence of the prior rate estimation. All values between the lower and upper uncertainty limits are equally likely.

In the applied Bayesian framework, the posterior joint and marginal PDFs of parameters and model predictions can be constructed from the sampling results. Standard deviations (σ) of marginal parameter PDFs are given in Table 2 as the uncertainties of rate rules. A 95% confidence interval of distributions is employed to indicate the model prediction uncertainties [46]. The large number of measurements and their small uncertainties strongly constrain the uncertainties of rate rules and thus also the model prediction uncertainties. For the most studied cases, the 95% confidence interval of prediction distributions corresponds to an uncertainty in the range of 0.5–

1
2
3
4
5
6
7
8
9 5%. The prediction uncertainties of ignition delay times for C₇–C₁₁ normal
10 alkanes are shown in the Supplementary material.
11
12

13 With the aid of the UQ framework, the knowledge about rate rules is
14 updated by extracting information from experimental data of *n*-heptane, *n*-
15 octane, *n*-nonane, *n*-decane, and *n*-undecane. As expected, these optimized
16 common rate rules demonstrate their capability to improve the model per-
17 formance for the fuels considered in the calibration.
18
19
20
21
22

23 4.4. Data consistency 24

25 While most experiments are well reproduced by the optimized model, the
26 constant pressure auto-ignition of *n*-heptane at a pressure of 6.5 atm [59]
27 appears as an outlier. In Fig. 8, the unoptimized model predicts the to-
28 tal ignition delay times measured with the novel CRV technique reasonably
29 well, but substantially underpredicts the first stage ignition data. After the
30 model optimization, the computed first stage ignition delay times appear
31 satisfactory for the conditions studied, while the entire ignition delays are
32 now overpredicted. To gain more insight into this, the prior 2D joint PDFs
33 of several prediction targets are presented in Fig. 9 in form of kernel density
34 estimation (KDE). Details of these targets are summarized in Table 3 as well
35 as in Figs. 8 and 10. A Monte Carlo sampling algorithm is used to determine
36 the error distribution of prediction targets. Random samples are generated
37 to represent the rate parameters according to their specified prior PDFs. For
38 each sample of the parameter set, targets are calculated for all conditions
39 of interest. This leads to an ensemble of prediction values that can be used
40 to estimate the joint distribution of prediction targets. The joint PDF ex-
41 plores how changing the value of a rate parameter requires other parameters
42
43
44
45
46
47
48
49
50
51
52
53
54
55
56
57
58
59
60
61
62
63
64
65

1
2
3
4
5
6
7
8
9
10
11
12
13
14
15
16
17
18
19
20
21
22
23
24
25
26
27
28
29
30
31
32
33
34
35
36
37
38
39
40
41
42
43
44
45
46
47
48
49
50
51
52
53
54
55
56
57
58
59
60
61
62
63
64
65

Class	Rate rules	Uncertainties (lower, upper)	A ₀	A*	n	E	σ*
			[cm ³ ,s,mol,K]	[cm ³ ,s,mol,K]	[-]	[cal/mol]	
C1	Fuel decomposition → H and alkyl radical	[4.0, 4.0]	1.000×10 ¹⁴	4.048×10 ¹³	0.00	0	0.0395
C1	Fuel decomposition → CH ₃ and alkyl radical	[4.0, 4.0]	1.000×10 ¹³	4.454×10 ¹²	0.00	0	0.0297
C1	Fuel decomposition → alkyl radicals	[4.0, 4.0]	8.000×10 ¹²	1.774×10 ¹³	0.00	0	0.0783
C2	H-atom abstraction from the fuel by H (primary carbon sites)	[4.0, 4.0]	2.220×10 ⁰⁵	2.922×10 ⁰⁵	2.54	6756	0.0675
C2	H-atom abstraction from the fuel by H (secondary carbon sites)	[4.0, 4.0]	6.500×10 ⁰⁵	1.635×10 ⁰⁵	2.40	4471	0.0339
C2	H-atom abstraction from the fuel by OH (P ₁)	[1.4, 1.4]	4.553×10 ⁰⁶	6.422×10 ⁰⁶	1.81	868	0.0129
C2	H-atom abstraction from the fuel by OH (S ₀₁)	[1.3, 1.3]	3.528×10 ⁰⁹	2.780×10 ⁰⁹	0.94	505	0.0231
C2	H-atom abstraction from the fuel by OH (S ₁₁)	[1.4, 1.4]	2.860×10 ⁰⁶	3.950×10 ⁰⁶	1.81	-1016	0.0125
C2	H-atom abstraction from the fuel by OH (S _{11'})	[1.6, 1.6]	2.810×10 ¹¹	1.761×10 ¹¹	0.32	847	0.0202
C2	H-atom abstraction from the fuel by HO ₂ (primary carbon sites)	[4.0, 4.0]	6.800×10 ⁰⁰	6.627×10 ⁰⁰	3.59	17160	0.0831
C2	H-atom abstraction from the fuel by HO ₂ (secondary carbon sites)	[4.0, 4.0]	3.160×10 ⁰¹	1.258×10 ⁰²	3.37	13720	0.0410
C2	H-atom abstraction from the fuel by CH ₃ (secondary carbon sites)	[4.0, 4.0]	7.550×10 ⁻⁰¹	3.718×10 ⁻⁰¹	3.46	5481	0.0287
C2	H-atom abstraction from the fuel by O ₂ (primary carbon sites)	[4.0, 4.0]	1.000×10 ¹³	5.942×10 ¹²	0.00	52290	0.0477
C2	H-atom abstraction from the fuel by O ₂ (secondary carbon sites)	[4.0, 4.0]	1.000×10 ¹³	1.338×10 ¹³	0.00	49640	0.0585
C2	H-atom abstraction from the fuel by C ₂ H ₅ (secondary carbon sites)	[4.0, 4.0]	2.500×10 ¹⁰	1.279×10 ¹⁰	0.00	10400	0.0637
C2	H-atom abstraction from the fuel by CH ₃ O ₂ (secondary carbon sites)	[4.0, 4.0]	5.090×10 ⁰⁹	2.442×10 ⁰⁹	3.58	14810	0.0695
C3	Alkyl radical (R) decomposition → alkene and H (primary carbon sites)	[4.0, 4.0]	4.240×10 ¹¹	2.220×10 ¹¹	0.51	1230	0.0474
C3	Alkyl radical (R) decomposition → alkene and H (secondary carbon sites)	[4.0, 4.0]	2.500×10 ¹¹	1.636×10 ¹¹	0.51	2620	0.0550
C3	Alkyl radical (R) decomposition → CH ₃ and alkene	[4.0, 4.0]	9.550×10 ⁰⁹	2.651×10 ⁰⁹	1.08	29388	0.1330
C3	Alkyl radical (R) decomposition → C ₂ H ₄ and alkyl radical	[4.0, 4.0]	9.120×10 ¹¹	3.579×10 ¹²	0.31	27238	0.0120
C3	Alkyl radical (R) decomposition → alkyl radical and alkene	[4.0, 4.0]	6.000×10 ¹¹	1.029×10 ¹²	0.50	27650	0.0464
C4	Alkyl radical (R) isomerization (5 member ring, secondary to primary carbon sites)	[4.0, 4.0]	3.460×10 ⁰⁰	1.401×10 ⁰⁰	3.20	16558	0.0190
C4	Alkyl radical (R) isomerization (5 member ring, secondary to secondary carbon sites)	[4.0, 4.0]	7.100×10 ⁻⁰¹	1.734×10 ⁰⁰	3.32	16140	0.0532
C4	Alkyl radical (R) isomerization (6 member ring, secondary to primary carbon sites)	[4.0, 4.0]	9.100×10 ⁰¹	3.295×10 ⁰²	2.55	10960	0.0217
C4	Alkyl radical (R) isomerization (6 member ring, secondary to secondary carbon sites)	[4.0, 4.0]	9.310×10 ⁻⁰¹	1.457×10 ⁰⁰	3.27	13200	0.0458
C4	Alkyl radical (R) isomerization (7 member ring, secondary to primary carbon sites)	[4.0, 4.0]	1.480×10 ⁰⁰	1.941×10 ⁰⁰	3.08	11020	0.0401
C5	H-atom abstraction from alkene by H	[4.0, 4.0]	1.040×10 ⁰⁷	5.019×10 ⁰⁶	2.400	4471	0.0245
C5	H-atom abstraction from alkene by OH	[4.0, 4.0]	3.740×10 ⁰⁸	2.406×10 ⁰⁸	1.610	-35	0.0751
C5	H-atom abstraction from alkene by HO ₂	[4.0, 4.0]	5.060×10 ⁰²	2.347×10 ⁰²	3.370	13720	0.0573
C8	Alkenyl radical decomposition → alkene and allyl (C ₃ H ₅)	[4.0, 4.0]	2.500×10 ¹³	1.222×10 ¹³	0.00	25000	0.0226
C9	Alkene decomposition	[4.0, 4.0]	2.500×10 ¹⁶	5.344×10 ¹⁶	0.00	71000	0.0309
C11	Addition of O ₂ to alkyl radicals (R) (primary carbon sites)	[2.2, 1.7]	1.301×10 ¹¹	8.898×10 ¹⁰	0.23	-1580	0.0252
C11	Addition of O ₂ to alkyl radicals (R) (secondary carbon sites)	[1.7, 2.1]	1.507×10 ¹⁵	1.039×10 ¹⁵	-0.92	-130	0.0238
C13	R + HO ₂ → RO + OH	[4.0, 4.0]	7.000×10 ¹²	1.227×10 ¹³	0.00	-1000	0.0442
C15	Alkyl peroxy radical isomerization (5 member ring, secondary carbon sites)	[3.1, 4.2]	2.327×10 ⁰⁷	1.506×10 ⁰⁷	1.40	28660	0.0839
C15	Alkyl peroxy radical isomerization (6 member ring, primary carbon sites)	[2.7, 2.5]	5.869×10 ⁰⁸	5.680×10 ⁰⁸	0.78	21850	0.0446
C15	Alkyl peroxy radical isomerization (6 member ring, secondary carbon sites)	[2.3, 2.2]	8.204×10 ¹⁰	5.010×10 ¹⁰	0.13	19470	0.0352
C15	Alkyl peroxy radical isomerization (7 member ring, secondary carbon sites)	[2.3, 1.6]	7.054×10 ⁰⁸	3.079×10 ⁰⁸	1.00	21070	0.0142
C15	Alkyl peroxy radical isomerization (8 member ring, secondary carbon sites)	[3.6, 1.4]	1.143×10 ¹⁰	1.357×10 ¹⁰	0.04	19780	0.0540
C16	Concerted eliminations (RO ₂ → alkene + HO ₂)	[2.2, 2.8]	2.885×10 ⁰⁹	6.650×10 ⁰⁹	0.93	29800	0.0201
C23	QOOH → cyclic ether + OH (3 member ring)	[3.3, 3.4]	2.282×10 ⁰⁸	1.389×10 ⁰⁸	1.29	9890	0.0354
C23	QOOH → cyclic ether + OH (4 member ring)	[11.1, 35.8]	4.579×10 ¹⁵	6.130×10 ¹⁵	-1.08	18440	0.0450
C23	QOOH → cyclic ether + OH (5 member ring)	[6.2, 7.4]	3.502×10 ¹⁰	6.974×10 ⁰⁹	0.10	9330	0.1120
C23	QOOH → cyclic ether + OH (6 member ring)	[4.0, 4.3]	3.553×10 ⁰⁷	9.621×10 ⁰⁷	0.69	10970	0.0348
C24	QOOH → alkene + HO ₂	[3.3, 2.4]	1.829×10 ¹⁰	1.016×10 ¹⁰	0.79	15100	0.0539
C25	QOOH → β-Scission products	[6.0, 8.5]	5.819×10 ⁰⁵	1.319×10 ⁰⁶	2.40	22790	0.0414
C26	Addition of O ₂ to QOOH (primary carbon sites)	[4.0, 4.0]	6.505×10 ¹⁰	1.034×10 ¹¹	0.23	-1580	0.0974
C26	Addition of O ₂ to QOOH (secondary carbon sites)	[4.0, 4.0]	7.535×10 ¹⁴	4.449×10 ¹⁴	-0.92	-130	0.0083
C27	Isomerization of O ₂ QOOH (6 member ring, primary OOH and secondary OO sites)	[4.0, 4.0]	5.489×10 ⁰³	2.628×10 ⁰³	2.40	19900	0.0494
C27	Isomerization of O ₂ QOOH (6 member ring, secondary OOH and secondary OO sites)	[4.0, 4.0]	1.754×10 ⁰²	4.471×10 ⁰²	3.10	17500	0.0326
C27	Isomerization of O ₂ QOOH (7 member ring, secondary OOH and secondary OO sites)	[4.0, 4.0]	2.536×10 ⁰²	1.184×10 ⁰²	2.60	16200	0.0493
C27	Isomerization of O ₂ QOOH (8 member ring, secondary OOH and primary OO sites)	[4.0, 4.0]	1.995×10 ⁰³	7.775×10 ⁰³	1.90	14900	0.0321
C28	Decomposition of carbonylhydroperoxide	[4.0, 4.0]	1.000×10 ¹⁶	6.065×10 ¹⁵	0.00	3900	0.0359
C29	Cyclic ether reactions with OH	[4.0, 4.0]	2.500×10 ¹²	1.045×10 ¹²	0.00	0	0.0492
C29	Cyclic ether reactions with HO ₂	[4.0, 4.0]	5.000×10 ¹²	1.988×10 ¹³	0.00	17700	0.0113
C30	H-atom abstraction from aldehyde by OH	[4.0, 4.0]	2.690×10 ¹⁰	3.582×10 ¹⁰	0.76	-340	0.0491
C31	Alternative isomerization of O ₂ QOOH (6 member ring, secondary carbon sites)	[4.0, 4.0]	8.204×10 ¹⁰	1.233×10 ¹¹	0.13	19470	0.0620

Table 2: Unoptimized and optimized rate rules; per H-atom basis. The lower and upper limits are the prior uncertainty limits. σ* denote the standard deviation of optimized rate rules.

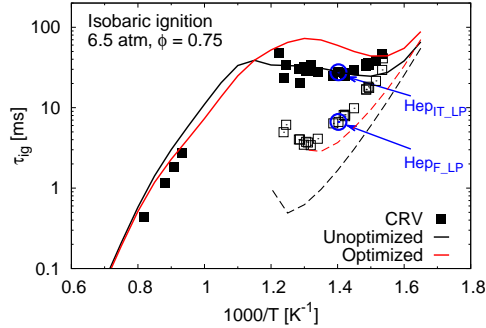


Figure 8: Ignition delay times of *n*-heptane/15%O₂/5%CO₂/Ar mixtures. Solid and open symbols denote the experimental total and first stage ignition delay times, respectively [59]. Solid and dashed lines show the numerical results for the total and first stage ignition delay times, respectively. Details on the circled points are provided in the main text.

to change in order to still yield acceptable predictions. If, for example, the joint PDF covers a wide area (e. g. as shown in Fig. 9(a)), then both predicted quantities can vary in their uncertainty limits independently. In other words, within the specified or determined uncertainties of the rate coefficients, there are probable combinations of rate parameters for independent variations of predicted ignition delays. If, however, the domain of the joint PDF covers a narrow region (e. g. in Fig. 9(b)), the change of rate parameters within the uncertainties would always lead to joint change in both predicted ignition delays.

It is interesting to observe in Fig. 9(a) that the first stage ignition delay times (Case Hep_{F,LP}) and the total ignition delay times (Case Hep_{IT,LP}) for *n*-heptane at 6.5 atm and 753 K are only weakly correlated. This allows for the possibility of increasing the first stage ignition delay time and simultaneously leaving the total ignition delay time unchanged in the model calibration.

Case	Fuel	Condition	Ignition delay
Hep _{IT_HP}	<i>n</i> -heptane	740 K, 13.5 bar, $\phi = 1.0$	Total
Hep _{LT_HP}	<i>n</i> -heptane	667 K, 13.5 bar, $\phi = 1.0$	Total
Hep _{IT_LP}	<i>n</i> -heptane	713 K, 6.5 atm, $\phi = 0.75$	Total
Hep _{F_LP}	<i>n</i> -heptane	713 K, 6.5 atm, $\phi = 0.75$	First stage
Dec _{LT_HP}	<i>n</i> -decane	734 K, 50.0 atm, $\phi = 1.0$	Total

Table 3: Calibration cases.

However, this is not observed after the calibration. The reason here lies in the strong correlation of Case Hep_{IT_LP} with cases at intermediate temperatures, e. g. Case Hep_{IT_HP}, as demonstrated in Fig. 9(b). In Fig. 10, an increased ignition delay time is observed for Case Hep_{IT_HP} after the calibration. Due to the strong correlation between these two cases, the total ignition delay time of Case Hep_{IT_LP} is inevitably increased.

Case Hep_{LT_HP} describes the auto-ignition of *n*-heptane at 667 K and 13.5 bar. At this condition, a large temperature rise is observed after the first stage auto-ignition, which enables a rapid consumption of ketohydroperoxide and results in a very short second stage induction. The first stage ignition delay time is thus almost identical to the total ignition delay time. As shown in Fig. 9, this case is strongly correlated with Case Hep_{F_LP}, as the ignition delay times at both conditions are mainly affected by the low temperature oxidation chemistry. Case Dec_{LT_HP} is also connected with Case Hep_{F_LP}, even though Case Dec_{LT_HP} presents the oxidation of *n*-decane at a very high pressure of 50 atm. As the initial temperature of Case Dec_{LT_HP} is relatively low, the prediction of the ignition delay time is again only sensitive to low

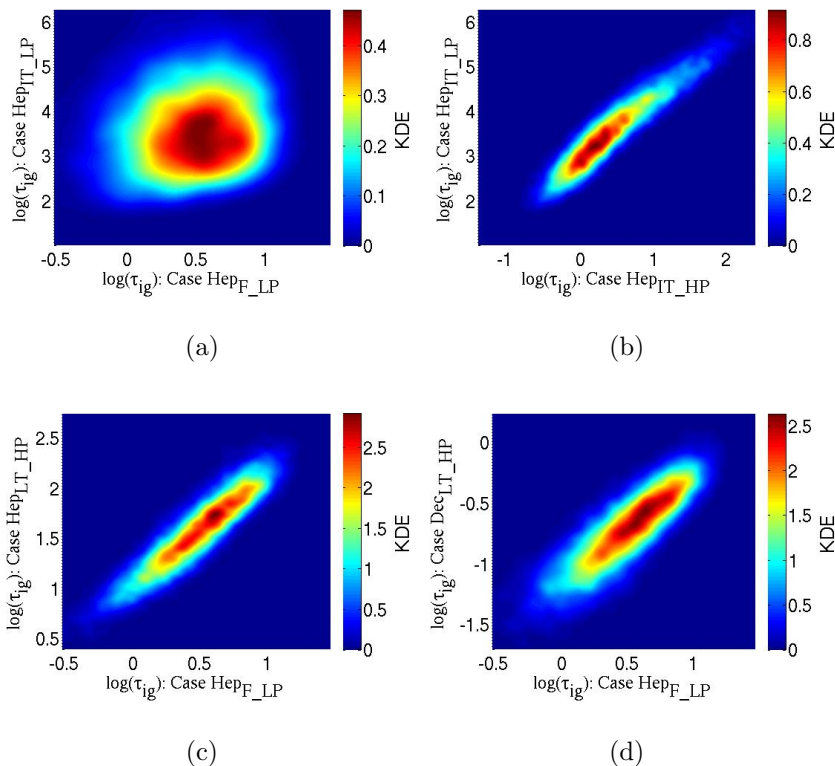


Figure 9: 2D prior joint PDFs of prediction targets. The log values of these prediction targets are presented.

temperature pathways. Moreover, common rate rules are used here for both n -heptane and n -decane. Due to these two facts, a strong correlation is established between Case Dec_{LT,HP} and Case Hep_{F,LP}.

4.5. Base chemistry

In the current model development procedure, a well-studied C₀–C₄ kinetic mechanism is taken as the base mechanism to describe the oxidation of intermediate species [8]. Its accuracy is of particular importance for the prediction of species profiles and burning velocities. Therefore, the effect of the

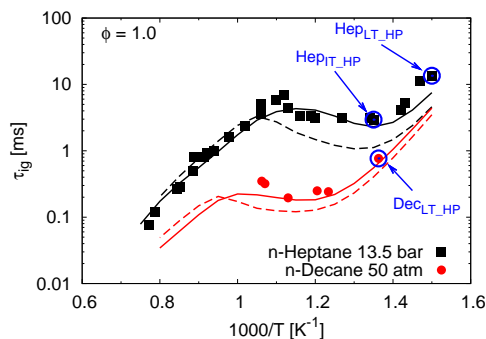


Figure 10: Ignition delay times of *n*-heptane/air and *n*-decane/air mixtures. Solid symbols denote experimental measurements [58, 60]. Solid lines show the numerical results for the present optimized model, and dashed lines show the results for the unoptimized model. Details on the circled points are provided in the main text.

base chemistry on the application and calibration of rate rules is evaluated in the following.

The base mechanism in the optimized model was replaced by the one from Narayanaswamy et al. [43] without alterations in the fuel specific chemistry. The numerical results of *n*-octane ignition delay times using that base mechanism (referred to as “Narayanaswamy”) are shown in Fig. 11, along with those computed with the optimized mechanism. For all conditions numerically studied, both models yield almost identical results. The calibration of rate rules is hence, at least in this example, independent of the base chemistry, which has often been assumed in past studies [5–11]. Regardless of the chosen base mechanism, identical reaction classes and rate rules have typically been employed to derive the fuel specific chemistry in various mechanisms. Nevertheless, it should be mentioned again that, even though the calibration and application of rate rules are not sensitive to the base chemistry, the

choice of the base mechanism is still of great importance. For example, the prediction of flame speeds depends solely on the reactions involved in the base mechanism [10].

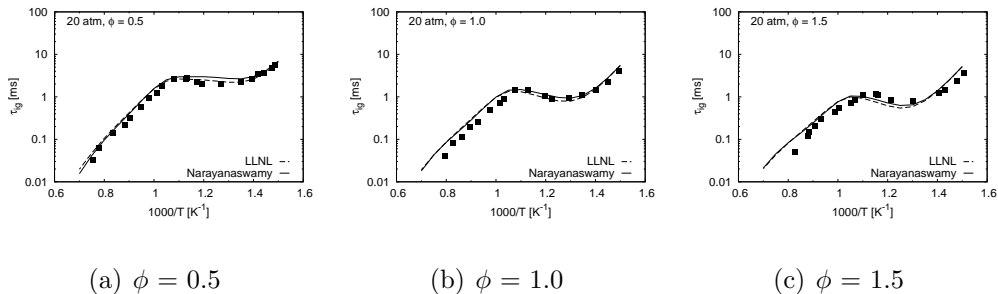


Figure 11: Ignition delay times of *n*-octane/air mixtures. Symbols denote experimental measurements [8]. Solid lines show numerical results for the base model from Narayanaswamy et al. [43], and dashed lines show the results for the base model from Sarathy et al. [8].

5. Mechanism development using optimized rate rules

This section explores how the optimized rate rules perform in the chemical mechanisms for larger alkanes that were not a part of the training set. *n*-Dodecane is chosen as the test case here, since data from various experimental configurations are available for this fuel, which enables an extensive validation of the developed model. In the following, an *n*-dodecane mechanism was derived using the rate rules calibrated in the previous section. This mechanism is compared with experimental measurements, a well-validated mechanism from the published literature [43], and a mechanism developed with the rate rules suggested in Refs. [8, 27, 56]. This allows for the assessment of the reliability and predictive quality of the optimized rate rules.

1
2
3
4
5
6
7
8
9 Two kinetic mechanisms were developed here for the combustion of n -dodecane.
10 Consistent with the model development process in Section 3, the n -dodecane
11 part in the LLNL mechanism [8] served as the starting point and was up-
12 dated according to Bugler et al. [27] and Sivaramakrishnan and Michael [56].
13 This proposed mechanism includes the up-to-date kinetic knowledge and the
14 rate rules [8, 27, 56] prior to the optimization. By replacing the unoptimized
15 rate rules with those optimized in Section 4, the second n -dodecane mech-
16 anism was generated. Figure 12 shows the numerical results for these two
17 mechanisms. The application of the optimized rate rules results in a signifi-
18 cant improvement of model performance for the entire range of temperatures.
19 **The prediction uncertainties of the mechanism with the optimized rate rules**
20 **are shown in the Supplementary material. The uncertainties were calculated**
21 **based on the Monte Carlo method with the samplings generated during the**
22 **UQ process. Detailed information for this calculation can be found in the**
23 **Supplementary material.**
24
25
26
27
28
29
30
31
32
33
34
35
36
37

38 In Fig. 13, the n -dodecane mechanism using the optimized rate rules is
39 compared with a well-validated mechanism recently published by Narayanaswamy
40 et al. [43]. The mechanism [43] was developed based on an extensive valida-
41 tion against measurements for various experimental configurations. However,
42 the new mechanism based on the optimized rate rules shows more accurate
43 predictions compared to the experimental data. More importantly, the mod-
44 ified mechanism reflects correctly the influence of equivalence ratio on the
45 ignition delays in the low temperature range. The strongly reduced ignition
46 delay times at low temperatures for n -dodecane are a major improvement and
47 where also expected as reported by Pei et al. [70], who stated that the models
48
49
50
51
52
53
54
55
56
57
58
59
60
61
62
63
64
65

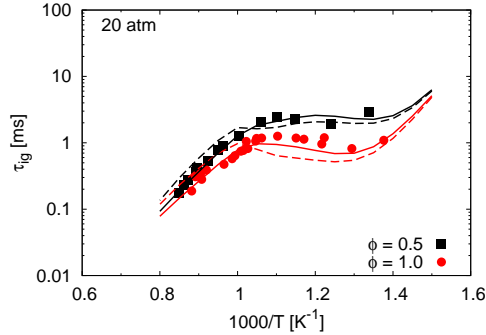


Figure 12: Ignition delay times of *n*-dodecane/air mixtures. Symbols denote experimental measurements [71]. Solid lines show the results for the model developed with the optimized rate rules, and dashed lines show the results for the model with the unoptimized rate rules [8, 27].

available in the literature ignite comparatively slowly in CFD simulations for spray experiments.

Additional comparison cases between the two models are presented in Figs. 14–19. Figures 14 and 15 show the concentrations of stable species measured in pressurized flow reactor configurations for stoichiometric *n*-dodecane/O₂/N₂ mixtures [72] and for lean *n*-dodecane/air mixtures [73], respectively. The discrepancies between experiment and simulation shown in Fig. 15 are mainly linked to the base chemistry, as analyzed in Ref. [43]. Malewicki and Brezinsky [74] measured the mole fractions of species for the oxidation of *n*-dodecane in a high pressure shock tube. The profiles of the reactants *n*-dodecane and O₂ are presented in Fig. 16, along with the data for some intermediate species, e.g. methane and acetylene. Figures 17 and 18 show the measurements for the pyrolysis of *n*-dodecane [74] and the oxidation of diluted *n*-dodecane/O₂/argon mixtures [75]. Discrepancies between

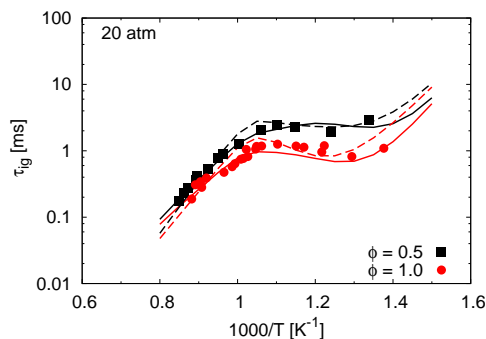


Figure 13: Ignition delay times of *n*-dodecane/air mixtures. Symbols denote experimental measurements [71]. Solid lines show the results for the model developed with the optimized rate rules, and dashed lines show the results for the model from Narayanaswamy et al. [43].

the model and the highly diluted oxidation measurements obtained at low pressures and high temperatures can be attributed to the fact that data under similar conditions for other *n*-alkanes were not utilized in the optimization process for rate rules. Data obtained under these conditions are primarily sensitive to unimolecular fuel decomposition reactions [76], which were not significantly optimized in the present work. The stable species concentration profiles during the oxidation of *n*-dodecane were measured in a jet stirred reactor by Ahmed et al. [69]. These data are shown in Fig. 19 in comparison with the simulation results. While the rate rules are optimized against shock tube measurements, data from various experimental configurations are taken into account here. For the most cases, the model with the optimized rate rules shows better agreement with experimental data.

The newly developed *n*-dodecane mechanism with the optimized rate rules gives satisfactory results. This is because the rate rules optimized based on experimental data of C_7 – C_{11} normal alkanes inherently capture the

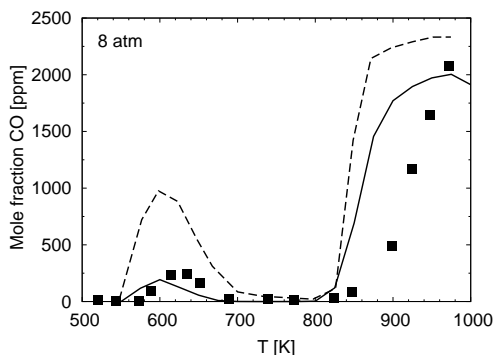


Figure 14: CO profiles of *n*-dodecane/O₂/N₂ (250/4625/995125 ppm) mixture combustion in a pressurized flow reactor at 8 atm with a residence time of 1 s. Symbols denote experimental measurements [72]. Solid lines show the results for the model developed with the optimized rate rules, and dashed lines show the results for the model from Narayanaswamy et al. [43].

analogous chemical kinetic features of *n*-dodecane. Therefore, the similarity in global oxidation behavior *n*-alkanes can be utilized to extract knowledge from shorter *n*-alkanes to benefit the development of kinetic models for longer *n*-alkanes such as *n*-dodecane. It is clearly demonstrated here that optimized rate rules improve the model performance when applied to derive models for larger hydrocarbons.

6. Concluding remarks

In this study, optimized rate rules for model development of normal alkanes are proposed. A chemical mechanism for C₇–C₁₁ *n*-alkanes was first developed by updating a published mechanism [8] according to the suggestions of Bugler et al. [27]. The resulting mechanism uses consistent rate rules for all of these fuels. It was then subjected to an automatic model

1
2
3
4
5
6
7
8
9
10
11
12
13
14
15
16
17
18
19
20
21
22
23
24
25
26
27
28
29
30
31
32
33
34
35
36
37
38
39
40
41
42
43
44
45
46
47
48
49
50
51
52
53
54
55
56
57
58
59
60
61
62
63
64
65

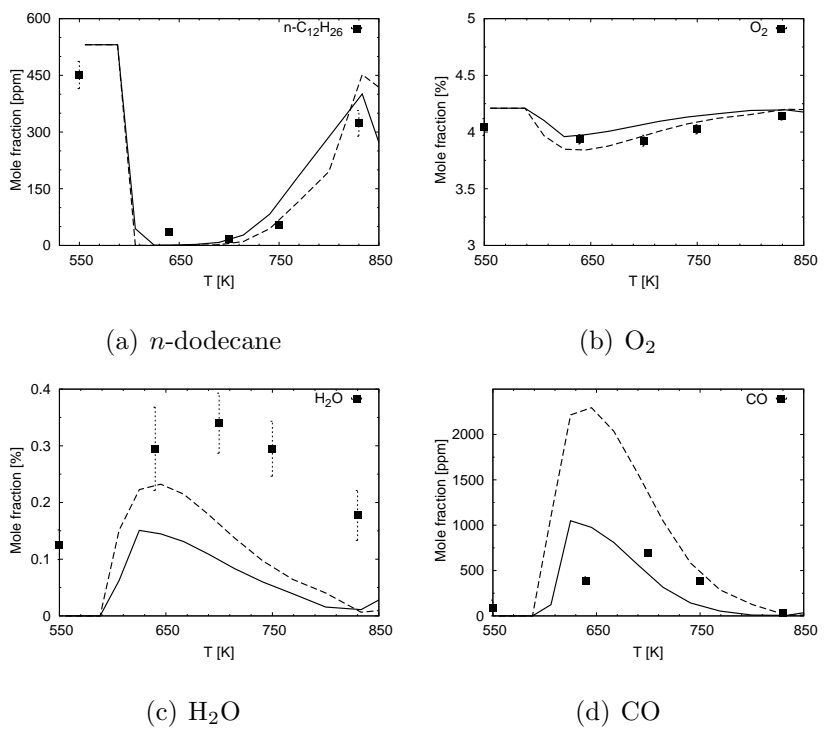


Figure 15: Stable species profiles of lean ($\phi = 0.23$) oxidation of *n*-dodecane/air mixtures in a pressurized flow reactor at 8 atm with a residence time of 0.12 s. Symbols denote experimental measurements [73]. Solid lines show the results for the model developed with the optimized rate rules, and dashed lines show the results for the model from Narayanaswamy et al. [43].

1
2
3
4
5
6
7
8
9
10
11
12
13
14
15
16
17
18
19
20
21
22
23
24
25
26
27
28
29
30
31
32
33
34
35
36
37
38
39
40
41
42
43
44
45
46
47
48
49
50
51
52
53
54
55
56
57
58
59
60
61
62
63
64
65

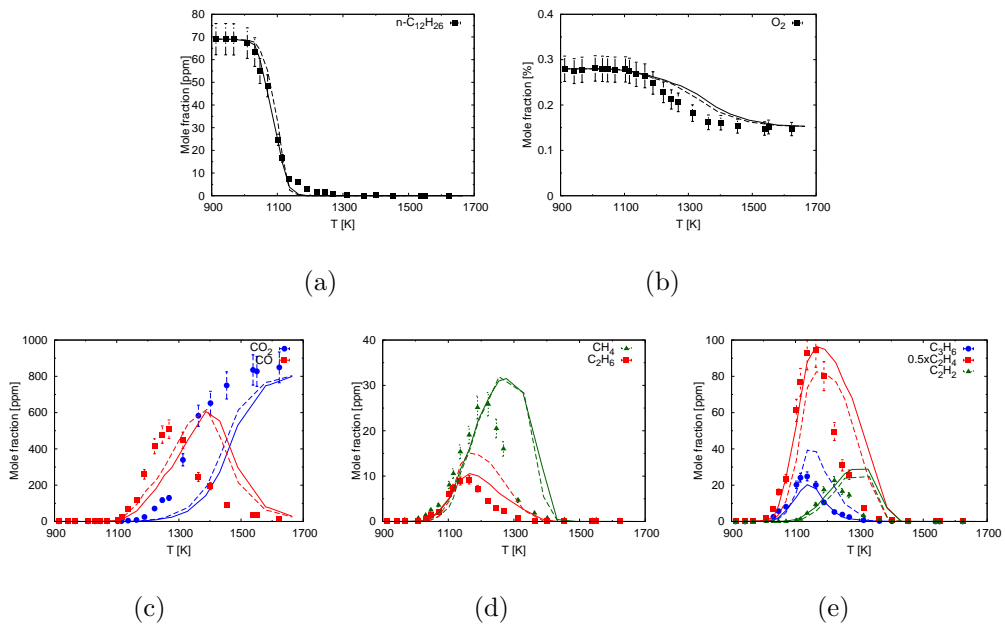


Figure 16: Stable species profiles of lean ($\phi = 0.46$) oxidation of *n*-dodecane/air mixtures in a shock tube at a pressure of 50 atm. Symbols denote experimental measurements [74]. Solid lines show the results for the model developed with the optimized rate rules, and dashed lines show the results for the model from Narayanaswamy et al. [43].

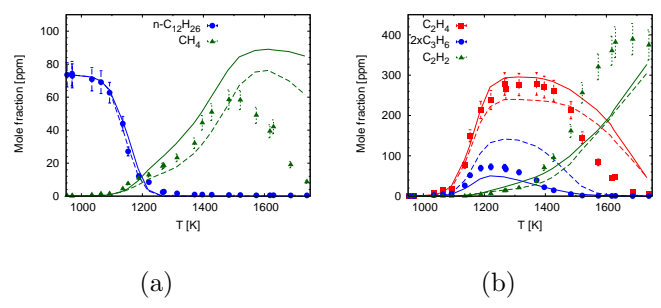


Figure 17: Stable species profiles of *n*-dodecane pyrolysis in a shock tube at a pressure of 22 atm [74]. Solid lines show the results for the model developed with the optimized rate rules, and dashed lines show the results for the model from Narayanaswamy et al. [43].

1
2
3
4
5
6
7
8
9
10
11
12
13
14
15
16
17
18
19
20
21
22
23
24
25
26
27
28
29
30
31
32
33
34
35
36
37
38
39
40
41
42
43
44
45
46
47
48
49
50
51
52
53
54
55
56
57
58
59
60
61
62
63
64
65

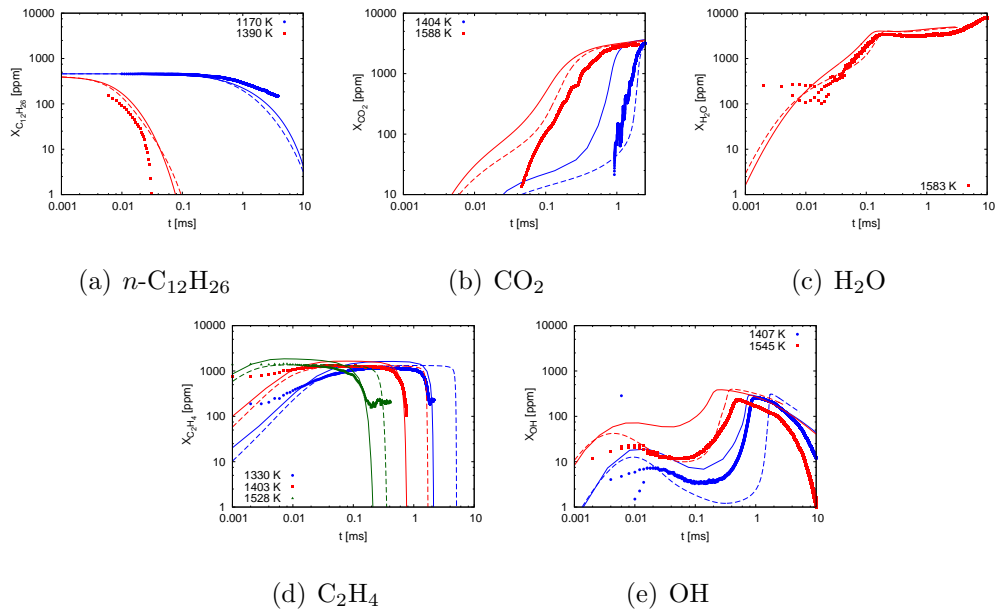


Figure 18: Species mole fractions of stoichiometric oxidation of *n*-dodecane/ O_2 /Ar mixtures in a shock tube at 2.25 atm. Symbols denote experimental measurements [75]. Solid lines show the results for the model developed with the optimized rate rules, and dashed lines show the results for the model from Narayanaswamy et al. [43].

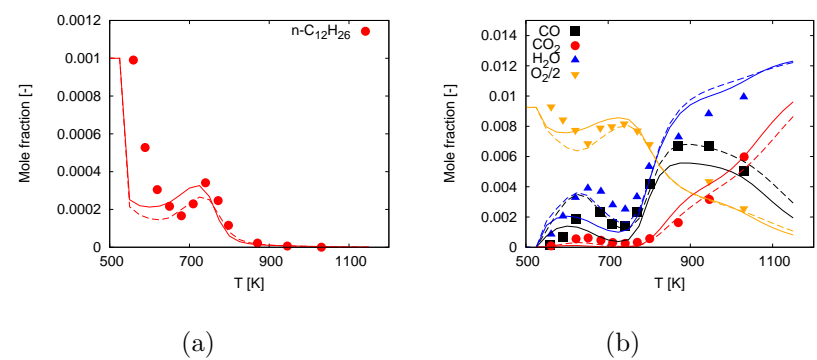


Figure 19: *n*-dodecane oxidation in a JSR at 10 bar, $\tau = 1.0$ s, and $\phi = 1.0$. The initial fuel mole fraction is 1000 ppm. Symbols denote the experimental data [69]. Solid lines show the results for the model developed with the optimized rate rules, and dashed lines show the results for the model from Narayanaswamy et al. [43].

1
2
3
4
5
6
7
8
9 optimization against a large number of experimental measurements, where
10 a Bayesian framework was applied to extract information from experiments
11 for different fuels to update the knowledge about rate rules. Excellent agree-
12 ment between simulations and experiments was achieved for the oxidation
13 of C₇–C₁₁ *n*-alkanes using the updated rate rules again consistently for all
14 fuels. After this successful training, the optimized rate rules were applied to
15 derive a chemical mechanism for *n*-dodecane, which was not used as part of
16 the training set. The proposed mechanism matches experimental data from
17 various experimental configurations over a variety of conditions well. Com-
18 pared with a mechanism using the unoptimized rate rules and a well-validated
19 mechanism from the published literature [43], the mechanism developed with
20 the calibrated rate rules shows substantially improved prediction accuracy.
21 Overall, it is demonstrated in the present study that the rate rules optimized
22 for a set of smaller hydrocarbon fuels are able to give satisfactory model
23 performance when applied in the model development for larger hydrocarbon
24 fuels.
25
26
27
28
29
30
31
32
33
34
35
36
37
38

39 This work presents a new approach for the development of chemical ki-
40 netic models, where models are first developed/updated using state-of-the-
41 art thermochemistry and reaction rate rules that draw from experiments and
42 theory-based computations. The combination of fundamental knowledge of
43 chemical kinetic modeling with information gained with the aid of uncertainty
44 quantification methods enables the development of more accurate chemical
45 kinetic models.
46
47
48
49
50
51
52
53
54
55
56
57
58

1
2
3
4
5
6
7
8
9
10
11
12
13
14
15
16
17
18
19
20
21
22
23
24
25
26
27
28
29
30
31
32
33
34
35
36
37
38
39
40
41
42
43
44
45
46
47
48
49
50
51
52
53
54
55
56
57
58
59
60
61
62
63
64
65

Acknowledgments

This work was performed within the Cluster of Excellence “Tailor-Made Fuels from Biomass”, which is funded by the Excellence Initiative of the German federal state governments to promote science and research at German universities. The authors also acknowledge funding support from the Clean Combustion Research Center and Saudi Aramco under the FUELCOM program. We would like to thank Dr. Krithika Narayanaswamy, Mr. Leif Kröger, and Mr. Christoph Thies for their support with numerical calculations and Dr. Sungwoo Park (KAUST) for his help with developing the kinetic model.

References

- [1] S. Honnet, K. Seshadri, U. Niemann, N. Peters, *Proc. Combust. Inst.* 32 (2009) 485-492
- [2] T. Malewicki, S. Gudiyella, K. Brezinsky, *Combust. Flame* 160 (2013) 17-30
- [3] H. Shen, J. Steinberg, J. Vanderover, M. Oehlschlaeger, *Energ Fuel* 23 (2009) 2482-2489
- [4] S.M. Sarathy, T. Javed, F. Karsenty, A. Heufer, W. Wang, S. Park, A. Elwardany, A. Farooq, C.K. Westbrook, W.J. Pitz, M.A. Oehlschlaeger, G. Dayma, H.J. Curran, P.Dagaut, *Combust. Flame* 161 (2014) 1444-1459

- 1
2
3
4
5
6
7
8
9 [5] H. Curran, P. Gaffuri, W. Pitz, C. Westbrook, *Combust. Flame* 114
10 (1998) 149-177
11
12
13 [6] H. Curran, P. Gaffuri, W. Pitz, C. Westbrook, *Combust. Flame* 129
14 (2002) 253-280
15
16
17
18 [7] C.K. Westbrook, W.J. Pitz, O. Herbinet, H.J. Curran, E.J. Silke, *Com-*
19 *bust. Flame* 156 (2009) 181-199
20
21
22 [8] S.M. Sarathy, C.K. Westbrook, M. Mehl, W. J. Pitz, C. Togbé, P. Da-
23 *gaut*, H. Wang, M.A. Oehlschlaeger, U. Niemann, K. Seshadri, P.S.
24 *Veloo*, C. Ji, F.N. Egolfopoulos, T. Lu, *Combust. Flame* 158 (2011)
25 2338-2357
26
27
28
29 [9] S.M. Sarathy, S. Vranckx, K. Yasunaga, M. Mehl, P. Oswald, W.K. Met-
30 *calfe*, C.K. Westbrook, W.J. Pitz, K. Kohse-Höinghaus, R.X. Fernandes,
31 *H.J. Curran*, *Combust. Flame* 159 (2012) 2028-2055
32
33
34 [10] L. Cai, A. Sudholt, D.J. Lee, F.N. Egolfopoulos, H. Pitsch, C.K. West-
35 *brook*, S.M. Sarathy, *Combust. Flame* 161 (2014) 798-809
36
37
38 [11] L. Cai, Y. Uygun, C. Togbé, H. Pitsch, H. Olivier, P. Dagaut, S.M.
39 *Sarathy*, *Proc. Combust. Inst.* 35 (2015) 419-427
40
41
42 [12] W.H. Green, J.W. Allen, R.W. Ashcraft, G.J. Beran, C.A. Class, C.
43 *Gao*, C.F. Goldsmith, M.R. Harper, A. Jalan, G.R. Magoon, D.M.
44 *Matheu*, S.S. Merchant, J.D. Mo, S. Petway, S. Raman, S. Sharma,
45 *J. Song*, K.M. Van Geem, J. Wen, R.H. West, A. Wong, H. Wong, P.E.
46 *Yelvington*, J. Yu, RMG Reaction Mechanism Generator Version 3.3,
47 <http://rmg.sourceforge.net/>.
48
49
50
51
52
53
54
55
56
57
58

1
2
3
4
5
6
7
8
9
10
11
12
13
14
15
16
17
18
19
20
21
22
23
24
25
26
27
28
29
30
31
32
33
34
35
36
37
38
39
40
41
42
43
44
45
46
47
48
49
50
51
52
53
54
55
56
57
58
59
60
61
62
63
64
65

[13] P.A. Glaude, F. Battin-Leclerc, R. Fournet, V. Warth, G.M. Côme, G. Scacchi, *Combust. Flame* 122 (2000) 451-462

[14] C. Zhou, J.M. Simmie, H.J. Curran, *Combust. Flame* 158 (2011) 726-731

[15] C. Zhou, J.M. Simmie, H.J. Curran, *Phys. Chem. Chem. Phys.* 12 (2010) 7221-7233

[16] S. Di Tommaso, P. Rotureau, O. Crescenzi, C. Adamo, *Phys. Chem. Chem. Phys.* 13 (2011) 14636-14645

[17] Z. Zhao, M. Chaos, A. Kazakov, F.L. Dryer. *Int. J. Chem. Kin.* 40 (1) (2008) 1-18

[18] A.V. Joshi, H. Wang. *Int. J. Chem. Kin.* 38 (2006) 57-73

[19] V. Vasudevan, D.F. Davidson, R.K. Hanson, *J. Phys. Chem. A.* 109 (2005) 3352-3359

[20] S.S. Vasu, Z. Hong, D.F. Davidson, R.K. Hanson, D.M. Golden, *J. Phys. Chem. A.* 114 (2010) 11529-11537

[21] R. Sivaramakrishnan, J.V. Michael, *Combust. Flame* 156 (2009) 1126-1134

[22] A. Miyoshi, *Int. J. Chem. Kin.* 44 (2012) 59-74

[23] S.M. Villano, L.K. Huynh, H.-H. Carstensen, A.M. Dean, *J. Phys. Chem. A* 115 (2011) 13425-13442

[24] S.M. Villano, L.K. Huynh, H.-H. Carstensen, A.M. Dean, *J. Phys. Chem. A* 116 (2012) 5068-5089

- 1
2
3
4
5
6
7
8
9 [25] A. Miyoshi, *J. Phys. Chem. A* 115 (2011) 3301-3325
10
11 [26] S. Sharma, S. Raman, W.H. Green, *J. Phys. Chem. A* 114 (2010) 5689-
12 5701
13
14
15 [27] J. Bugler, K.P. Somers, E.J. Silke, H.J. Curran, *J. Phys. Chem. A* 119
16 (2015) 7510-7527
17
18
19 [28] C.F. Goldsmith, W.H. Green, S.J. Klippenstein, *J. Phys. Chem. A* 116
20 (2012) 3325-3346
21
22
23 [29] L.K. Huynh, H.H. Carstensen, A.M. Dean, *J. Phys. Chem. A* 114 (2010)
24 6594-6607
25
26
27 [30] C.Y. Sheng, J.W. Bozzelli, A.M. Dean, A.Y. Chang, *J. Phys. Chem. A*
28 106 (2002) 7276-7293
29
30
31 [31] J.A. Miller, S.J. Klippenstein, S.H. Robertson, *Proc. Combust. Inst.* 28
32 (2000) 1479-1486
33
34
35 [32] J.A. Miller, S.J. Klippenstein, *Int. J. Chem. Kin.* 33 (2001) 654-668
36
37
38 [33] J.D. DeSain, S.J. Klippenstein, J.A. Miller, C.A. Taatjes, *J. Phys.*
39 *Chem. A* 107 (2003) 4415-4427
40
41
42 [34] H. Sun, J.W. Bozzelli, *J. Phys. Chem. A* 108 (2004) 1694-1711
43
44
45
46 [35] M. Frenklach, *Combust. Flame* 58 (1984) 69-72
47
48
49 [36] M. Frenklach, A. Packard, P. Seiler, R. Feeley, *Int. J. Chem. Kin.* 36
50 (2004) 57-66
51
52
53
54
55
56
57
58
59
60
61
62
63
64
65

1
2
3
4
5
6
7
8
9
10
11
12
13
14
15
16
17
18
19
20
21
22
23
24
25
26
27
28
29
30
31
32
33
34
35
36
37
38
39
40
41
42
43
44
45
46
47
48
49
50
51
52
53
54
55
56
57
58
59
60
61
62
63
64
65

[37] D.A. Sheen, H. Wang. *Combust. Flame* 158 (2011) 2358-2374

[38] M.T. Reagan, H.N. Najm, R.G. Ghanem, O.M. Knio. *Combust. Flame* 132 (3) (2003) 545-555

[39] H. Wang, D.A. Sheen, *Progress in Energy and Combustion Science* 47 (2015) 1-31

[40] L. Cai, H. Pitsch, *Combust. Flame* 161 (2014) 405-415

[41] M. Frenklach, D.W. Clary, *Twentieth Symposium (International) on Combustion* (1984) 887-901

[42] L. Cai, H. Pitsch, *Combust. Flame* 162 (2015) 1623-1637

[43] K. Narayanaswamy, P. Pepiot, H. Pitsch, *Combust. Flame* 161 (2014) 866-884

[44] R.T. Cox, *The Algebra of Probable Inference*, Johns Hopkins University Press, Baltimore, MD, (1961)

[45] E.T. Jaynes, *Probability Theory: The Logic of Science*, Cambridge University Press, Cambridge, (2003)

[46] K. Braman, T.A. Oliver, V. Raman, *Combustion Theory and Modelling* 17 (2013) 858-887

[47] J. Prager, H.N. Najm, K. Sargsyan, C. Safta, W.J. Pitz, *Combust. Flame* 160 (2013) 1583-1593

- 1
2
3
4
5
6
7
8
9 [48] E. Prudencio, K.W. Schulz, Workshop on Algorithms and Program-
10 ming Tools for Next-Generation High-Performance Scientific Software
11 (HPSS), Bordeaux, France, 2011
12
13
14
15 [49] S. Mosbach, J.H. Hong, G.P.E. Brownbridge, M. Kraft, S. Gudiyella, K.
16 Brezinsky, *Int. J. Chem. Kin.* 46 (2014) 389-404
17
18
19
20 [50] K. Miki, E.E. Prudencio, S.H. Cheung, G. Terejanu, *Combust. Flame.*
21 160 (2013) 861-869
22
23
24
25 [51] S. G. Davis, A. B. Mhadeshwar, D. G. Vlachos, H. Wang, *Int. J. Chem.*
26 *Kinet.* 36 (2004) 94-106
27
28
29
30 [52] H. Pitsch, FlameMaster: A C++ computer program for 0D combustion
31 and 1D laminar flame calculations
32
33
34 [53] S.M. Burke, J.M. Simmie, H.J. Curran, *J. Phys. Chem. Ref. Data* 44
35 (2015) 013101
36
37
38
39 [54] S.W. Benson, *Thermochemical Kinetics*, 2nd ed.; Wiley: New York
40 (1976)
41
42
43 [55] E.R. Ritter, J.W. Bozzelli, THERM: Thermodynamic Property Estima-
44 tion for Gas Phase Radicals and Molecules. *Int. J. Chem. Kin.* 23 (1991)
45 767-778
46
47
48
49
50 [56] R. Sivaramakrishnan, J.V. Michael, *J. Phys. Chem. A* 113 (2009) 5047-
51 5060
52
53
54
55 [57] P. Pepiot-Desjardins, H. Pitsch, *Combust. Flame*, 154 (2008) 67-81
56
57
58

- 1
2
3
4
5
6
7
8
9 [58] U. Pfahl, K. Fieweger, G. Adomeit, Proc. Combust. Inst. 26 (1996)
10 781-789
11
12
13 [59] M.F. Campbell, S. Wang, C.S. Goldenstein, R.M. Spearrin, A.M.
14 Tulgestke, L.T. Zaczek, D.F. Davidson, R.K. Hanson, Proc. Combust.
15 Inst. 35 (2015) 231-239
16
17
18
19 [60] H.K. Ciezki, G. Adomeit Combust. Flame 93 (1993) 421-433
20
21
22 [61] V.P. Zhukov, V.A. Sechenov, A.Yu. Starikovski, Combust. Flame 153
23 (2008) 130-136
24
25
26
27 [62] B. Rotavera, E.L. Petersen, Shock Waves 23 (2013) 345-359
28
29
30 [63] D.F. Davidson, S.C. Ranganath, K.-Y. Lam, M. Liaw, Z. Hong, R.K.
31 Hanson, J. Prop. Power (26) 2010
32
33
34 [64] A. Chakir, M. Bellimam, J.C. Boettner, Cathonnet, Int. J. Chem. Kin.
35 24 (1992) 385-410
36
37
38
39 [65] O. Herbinet, B. Husson, Z. Serinyel, M. Cord, V. Warth, R. Fournet, P.
40 Glaude, B. Sirjean, F. Battin-Leclerc, Z. Wang, M. Xie, Z. Cheng, F.
41 Qi, Combust. Flame 159 (2012) 3455-3471
42
43
44
45 [66] F.L. Dryer, K. Brezinsky, Combustion Science and Technology 45 (1986)
46 199-212
47
48
49
50 [67] S.P. Zeppieri, S.D. Klotz, F.L. Dryer, Proc. Combust. Inst. 28 (2000)
51 1587-1595
52
53
54
55 [68] G. Mittal, M.P. Raju, C.-J. Sung, Combust. Flame 157 (2010) 1316-1324
56
57
58

1
2
3
4
5
6
7
8
9
10
11
12
13
14
15
16
17
18
19
20
21
22
23
24
25
26
27
28
29
30
31
32
33
34
35
36
37
38
39
40
41
42
43
44
45
46
47
48
49
50
51
52
53
54
55
56
57
58
59
60
61
62
63
64
65

[69] A. Mz -Ahmed, K. Hadj-Ali, P. Dagaut, G. Dayma, *Energy Fuels* 26 (2012) 4253-4268

[70] Y. Pei, E.R. Hawkes, S. Kook, G.M. Goldin, T. Lu, *Combust. Flame* 162 (2015) 2006-2019

[71] S.S. Vasu, D.F. Davidson, Z. Hong, V. Vasudevan, R.K. Hanson, *Proc. Combust. Inst.* 32 (2009) 173-180

[72] P.S. Veloo, S. Jahangirian, F.L. Dryer, Spring Technical Meeting, Central States Section of the Combustion Institute (2012)

[73] M.S. Kurman, R.H. Natelson, N.P. Cernansky, D.L. Miller, *Proc. Combust. Inst.* 33 (2011) 159-166

[74] T. Malewicki, K. Brezinsky, *Proc. Combust. Inst.*, 34 (2013) 361-368

[75] D.F. Davidson, Z. Hong, G.L. Pilla, A. Farooq, R.D. Cook, R.K. Hanson, *Proc. Combust. Inst.* 33 (2011) 151-157

[76] S.S. Vasu, S.M. Sarathy, *Energy Fuels* 27 (2013) 7072-7080

Supplementary Material

[Click here to download Supplementary Material: Package_400.zip](#)

Supplementary Material

[Click here to download Supplementary Material: Readme](#)

Supplementary Material

[Click here to download Supplementary Material: supplementary.pdf](#)

Thermo data in FlameMaster format

[Click here to download Supplementary Material: nalkanes.thermo](#)

Transport data in FlameMaster format

[Click here to download Supplementary Material: nalkanes.trans](#)

Mechanism in FlameMaster format

[Click here to download Supplementary Material: nalkanes.mech](#)

Thermo data in Chemkin format

[Click here to download Supplementary Material: nalkanes.chthermo](#)

Mechanism in Chemkin format

[Click here to download Supplementary Material: nalkanes.chmech](#)

Transport data in Chemkin format

[Click here to download Supplementary Material: nalkanes.chtrans](#)